Characterization of Anti-Neovascularization Activity and Ocular Pharmacokinetics of PI3K/mTOR Inhibitor GNE-947

Xingrong Liu, Xiaorong Liang, Jenninfer LeCouter, Savita Ubhayakar, Jacob Chen, Jay Cheng, Tom Lee, Joe Lubach, Jim Nonomiya, Sheerin Shahidi-Latham, Cristine Quiason, Eric Solon[#], Matthew Wright, Cornelis E. C. A. Hop, and Timothy P. Heffron*

Genentech Inc., 1 DNA Way, South San Francisco, California 94080; [#]QPS, Delaware Technology Park 3 Innovation Way, Newark, Delaware 19711

Running title: Characterization of PI3K/mTOR Inhibitor GNE-947

Address correspondence to:

Timothy P. Heffron, Ph.D.

Genentech, Inc., 1 DNA Way, South San Francisco, CA 94080

TEL: (650) 467-3214, E-mail: heffron.timothy@gene.com

The number of text pages: 23

The number of tables: 5

The number of figures: 9

The number of references: 41

The number of words in abstract: 273

The number of words in introduction: 700

The number of words in discussion: 1589

Abbreviations: CNV, choroidal neovascular; HUVEC, human umbilical vein endothelial cell; LLOQ, lower limit of quantitation; MALDI, matrix assisted laser desorption/ionization; MRM, multiple reaction monitoring; mTOR, mammalian target of rapamycin; NV AMD, neovascular age related macular degeneration; PI3K, phosphoinositide 3-kinase; PDGF-B, platelet-derived growth factor B; PIKK, phosphatidyl inositol-like kinase; PIP3, 3,4,5-inositoltriphosphate; S1P, sphingosine-1-phosphate; VEGF, vascular endothelial growth factor.

Abstract

The objectives of the present study were to characterize GNE-947 for its phosphoinositide 3-kinase (PI3K) and mammalian target of rapamycin (mTOR) inhibitory activities, in vitro anti-cell migration activity in Human Umbilical Vein Endothelial Cells (HUVEC), in vivo anti-neovascularization activity in laser induced rat choroidal neovascular (CNV) eyes, pharmacokinetics in rabbit plasma and eyes, and ocular distribution using Matrix-Assisted Laser Desorption Ionization Imaging mass spectrometry (MALDI-IMS) and autoradioluminography. Its PI3K and mTOR Ki were 0.0005 µM and 0.045 µM, respectively, and its HUVEC IC_{50} was 0.093 µM. GNE-947 prevented neovascularization in the rat CNV model at 50 or 100 µg/eye with repeat dosing. Following a single intravenous injection at 2.5 and 500 µg/kg in rabbits, its plasma terminal half-lives ($t_{1/2}$) were 9.11 and 9.59 hours, respectively. Following a single intravitreal injection of a solution at 2.5 µg/eye in rabbits, its apparent $t_{1/2}$ values were 14.4, 16.3, and 23.2 hours in the plasma, vitreous humor, and aqueous humor, respectively. Following a single intravitreal injection of a suspension at 33.5, 100, 200 µg/eye in rabbits, the $t_{1/2}$ were 29, 74, and 219 days in the plasma; and 46, 143, and 191 days in the eyes, respectively. MALDI-IMS and autoradioluminography images show that GNE-947 did not homogenously distribute in the vitreous humor and aggregated at the injection sites following injection of the suspension, which was responsible for the long $t_{1/2}$ of the suspension due to slow dissolution process. This hypothesis was supported by pharmacokinetic modeling analyses. In conclusion, PI3K/mTOR inhibitor GNE-947 prevented neovascularization in a rat CNV model with $t_{1/2}$ up to approximately six months following a single intravitreal injection of the suspension in rabbit eyes.

Significance Statement

GNE-947 is a potent PI3K/mTOR inhibitor and exhibits anti-CNV activity in rat eyes. The duration of GNE-947 in the rabbit eyes following intravitreal injection in a solution is short with $t_{1/2}$ less than a day. However, the duration following intravitreal dose of a suspension is long with

$t_{1/2}$ up to six months due to low solubility and slow dissolution. These results indicate that intravitreal injection of a suspension for low solubility drugs can be used to achieve long-term drug exposure.

Introduction

Vascular endothelial growth factor (VEGF) is a potent, diffusible, endothelial-specific mitogen and a blood vessel permeability factor induced during the progression of intraocular vascular pathologies. It is a clinically validated anti-angiogenic and vascular permeability target in neovascular (wet) age related macular degeneration (NV AMD) (Ferrara et al. 2006; Miller et al. 2013). As such, VEGF neutralizing agents, including an antibody-based therapy such as ranibizumab (rhuFAb VEGF, Lucentis®; Genentech, Inc., South San Francisco, CA) and a VEGF decoy receptor and antibody fragment crystallizable-chimeric protein, aflibercept (VEGF-TRAPR1R2, VIEW1/2, Eylea®; Regeneron, Tarrytown, NY), are now used as standards in the clinical management of NV AMD and other ocular diseases including central retinal vein occlusion. Despite the clinical successes of currently available anti-VEGF therapies, there is still a significant unmet medical need in the treatment of NV AMD with respect to both maximizing the magnitude of visual gains and the durability of effects. Approximately 30% of patients had an improved best-corrected visual acuity of equal to or greater than 15 letters in pivotal clinical trials with ranibizumab (Chang et al. 2007; Bressler et al. 2009; Busbee et al. 2013) and aflibercept (Heier et al. 2012). The majority of patients in these studies did not achieve a 15-letter improvement in visual acuity and approximately 29% of patients continued to lose vision, suggesting that there are additional signaling pathways and/or mechanisms promoting pathological neovessel growth, leakage, and loss of retinal function in patients with NV AMD.

VEGF receptor 2 (VEGFR-2) is the tyrosine kinase receptor that signals VEGF-mediated endothelial cell growth, survival, vessel morphogenesis, and permeability (reviewed in Ferrara et al. 2003). VEGFR-2 signals primarily through the phosphatidyl inositol 3-kinase pathway (Gerber et al. 1998; Ferrara 1999). Specifically, the Class I PI3K kinases and mTOR kinase (a member of the PIKK, phosphatidyl inositol-like kinase, family) have been demonstrated to be

required for angiogenesis and vascular integrity in vivo (Hamada et al. 2005; Graupera et al. 2008; Schnell et al. 2008; Yuan et al. 2008; Sampath et al. 2013). GNE-947 is an inhibitor of the Class I PI3K kinases and the downstream mTOR kinase (Figure 1). This dual targeting permits a more potent VEGFR-2 pathway inhibition than more selective compounds and alleviates the feedback activation loop downstream of selective mTOR inhibitors (O'Reilly et al. 2006; Wallin et al. 2012).

In addition to VEGFR, the PI3K/mTOR pathway is used by many receptor systems implicated in NV AMD, including platelet-derived growth factor B (PDGF-B) and the bioactive lipid sphingosine-1-phosphate (S1P), suggesting that inhibiting PI3K/mTOR in the eye may have a broader therapeutic utility than only targeting VEGF (Jo et al. 2006; Caballero et al. 2009). Thus, GNE-947 may offer a single therapy to inhibit signaling from a spectrum of receptors clinically validated or implicated in NV AMD pathology.

Currently approved therapies for NV AMD require frequent intravitreal injections, 8−12 times per year, to maintain optimal efficacy and vision improvement. In trials evaluating fixed quarterly dosing versus monthly dosing of ranibizumab, patients assigned to the less frequent dosing groups gained fewer letters than patients dosed monthly (Regillo et al. 2008; Schmidt-Erfurth et al. 2011). The frequent dosing required for current therapies decreases patient adherence and increases the risk of injection-related complications. Our planned approach is to utilize PI3K pathway inhibitors for the treatment of retinal diseases focused on administration of a small molecule PI3K/mTOR inhibitor via intravitreal injection with an objective of needing to administer the PI3K inhibitor infrequently, ideally just once every 6 months.

We hypothesized that we could achieve such a long-acting PI3K inhibitor for retinal diseases by injecting a suspension of drug where limited solubility and dissolution would allow for sustained release. In the present work, we characterized the PI3K and mTOR biochemical potency, anti-

cell migration activity, in vivo anti-neovascularization activity in rat eyes, and plasma and ocular pharmacokinetics of GNE-947 following intravitreal injections of solution or suspension formulations in rabbits. We also used Matrix-Assisted Laser Desorption Ionization Imaging mass spectrometry (MALDI-IMS) and autoradioluminography to examine the ocular distribution and dissolution of GNE-947. The results from the present study are not only helpful in designing PI3K/mTOR inhibitors for treatment of wAMD but also will inform programs directed at the discovery of drugs to treat other retinal diseases.

Materials and Methods

Chemicals. Ten PI3K inhibitors (Table 1) were synthesized at Genentech (South San Francisco, CA) or Wuxi (Shanghai, China). $^{13}C^{15}N_3$-GNE-947 was synthesized by IsoSciences (King of Prussia, PA). ^{14}C-GNE-947 was synthesized by Selcia (Essex, UK). Synthetic melanin was obtained from Sigma-Aldrich (St. Louis, MI) with purity of 100%. All chemicals used in the experiments were of the highest available grade.

PI3K Inhibition. As previously published (Heffron et al. 2016), enzymatic activity of the Class I PI3K isoforms was measured using a fluorescence polarization assay that monitors formation of the product 3,4,5-inositoltriphosphate molecule (PIP3) as it competes with fluorescently labeled PIP3 for binding to the GRP-1 pleckstrin homology domain protein. An increase in phosphatidyl inositide-3-phosphate product results in a decrease in fluorescence polarization signal as the labeled fluorophore is displaced from the GRP-1 protein binding site. Class I PI3K isoforms were purchased from Perkin Elmer or were expressed and purified as heterodimeric recombinant proteins. Tetramethylrhodamine-labeled PIP3 (TAMRA-PIP3), di-C8-PIP2, and PIP3 detection reagents were purchased from Echelon Biosciences. PI3K isoforms were assayed under initial rate conditions in the presence of 10 mM Tris (pH 7.5), 25 µM ATP, 9.75 µM PIP2, 5% glycerol, 4 mM $MgCl_2$, 50 mM NaCl, 0.05% (v/v) Chaps, 1 mM dithiothreitol, 2% (v/v) DMSO at the following concentrations for each isoform: PI3Kα,β at 60 ng/mL; PI3Kγ at 8 ng/mL; PI3Kδ at 45 ng/mL. After incubation for 30 minutes at 25 °C, reactions were terminated with a final concentration of 9 mM EDTA, 4.5 nM TAMRA-PIP3, and 4.2 µg/mL GRP-1 detector protein before reading fluorescence polarization on an Envision plate reader. Apparent Ki values were determined at a fixed concentration of ATP near the measured Km for ATP for each isoenzyme, and were calculated by fitting of the dose-response curves to an equation for tight-binding competitive inhibition. All apparent Ki values represent geometric means of

minimum of three determinations. These assays generally produced results within 2-fold of the reported mean.

mTOR Inhibition. As previously published (Heffron et al. 2012), human recombinant mTOR (1360-2549) was expressed and purified from insect cells and assayed using a Lanthascreen fluorescence resonance energy transfer format from Invitrogen in which phosphorylation of recombinant green fluorescent protein (GFP)-4-EBP1 is detected using a terbium-labeled antibody to phospho-threonine 37/46 of 4-EBP1. Reactions were initiated with ATP and conducted in the presence of 50 Mm Hepes (pH 7.5), 0.25 nM mTOR, 400 nM GFP-4E-BP1, 8 μM ATP, 0.01% (v/v) Tween 20, 10 mM MnCl2, 1 mM EGTA, 1 mM dithiothreitol, and 1% (v/v) DMSO. Assays were conducted under initial rate conditions at room temperature for 30 min before terminating the reaction and detecting product in the presence of 2 nM Tb-anti-p4E-BP1 antibody and 10 mM EDTA. Dose-response curves were fit to an equation for competitive tight-binding inhibition and apparent Ki values were calculated using the determined Km for ATP of 6.1 μM. All apparent Ki values represent geometric means of minimum of two determinations. These assays generally produced results within 2-fold of the reported mean.

HUVEC Cell migration assay. Trans-well inserts (BD Bioscie**nc**es #353097) were coated overnight with 8 μg/ml fibronectin (Sigma #F1141). In vitro Human Umbilical Vein Endothelial Cells (HUVEC) (Lonza #CC-2519) were incubated in EBM basal medium (Lonza #CC-3121) containing 0.1% BSA for 6 hours in order to serum-starve the cells. HUVEC were then plated into the Trans-well inserts ($5x10^5$ cells/well) were then incubated overnight with or without 10 ng/mL VEGF and serially diluted PI3K inhibitors (in triplicate per concentration). Positive control for this experiment was cells cultured with 10ng/mL VEGF without PI3K inhibitors. Negative control were cells treated with 10 ng/mL VEGF and 10ng/mL anti-VEGF antibodies (Lucentis). Cells were then fixed with methanol and stained with Sytox Green (Invitrogen). Cells were on

the top of the plates were scraped and washed with PBS to remove cells that did not migrate. Nuclei on the bottom of the insert were counted to number of cells that migrated. The IC50 value was then calculated by plotting the PI3K inhibitor concentration against the percent cells migrated on a graph**.**

Solubility. Solubility of molecules was determined according to the method described by Lin and Pease (Lin 2016).

Plasma Protein Binding. Protein binding determination was conducted at 37°C by an equilibrium dialysis method using a Single-Use Plate Rapid Equilibrium Dialysis device with dialysis membranes with a molecular weight cut off of approximately 8,000 Da. Equilibrium dialysis was carried out using 0.3 mL of spiked plasma dialyzed against 0.5 mL of blank potassium phosphate buffer (pH=7.4) at 37°C for 6 hours. Samples were stored at approximately -20°C until analysis. GNE-947 concentrations in plasma/phosphate buffer were determined using an LC-MS/MS method.

Melanin Binding. Melanin binding was determined using a method reported previously (Koeberle et al., 2003). Briefly, 2 mL of melanin suspension at 1 mg/mL was sonicated for approximately 15 minutes and kept in a 37°C incubator for approximately 30 minutes prior to spiking with GNE-947. After stirred at 37°C for 180 minutes, 1.3 mL of the suspension was centrifuged at 280,000×g for 15 minutes. Then a 0.2 mL aliquot of supernatant was collected into a tube containing a mixture of 0.2 mL blank human plasma and 0.2 mL blank melanin suspension (1 mg/mL). Samples were stored at approximately -20°C until analysis. GNE-947 were determined using an LC-MS/MS method.

Intravenous Administration of GNE-947. The systemic pharmacokinetics of GNE-947 were evaluated following an intravenous single bolus administration of 2.5 (n=8) or 500 (n=4) µg/kg in male Dutch-Belted rabbits with average of body weight of 2 kg. The vehicle for 2.5 µg/kg

formulation was 10%PEG400 in phosphate buffered saline and the vehicle used for 500 µg/kg formulations was 20%Hydroxypropyl-β-Cyclodextrin/0.23% NaCl. Following intravenous administration at 1 mL/kg through ear vein, approximately 800 µL blood samples were collected from central ear artery at 5, 15 minutes, 1, 2, 4, 8, and 24 hours for the 2.5 µg/kg group and at 2, 5, 15, 30 min, 1, 2, 4, 8, and 24 hours for the 500 µg/kg. Blood samples were placed into tubes containing K_2EDTA. Blood samples were centrifuged at approximately 11,000 RPM for approximately 5 minutes at 4°C to obtain plasma. The plasma samples were stored at -80ºC before analysis. All studies were approved by Genentech Institutional Animal Care and Use Committee.

Intravitreal Administration of GNE-947 in Solution Formulation. The pharmacokinetics of GNE-947 were evaluated following intravitreal administration in male Dutch-Belted rabbits with average of body weight of 2 kg. The vehicle for intravitreal formulation was 10%PEG400 in phosphate buffered saline. The rabbits were anesthetized with intramuscular injection of 5 mg/kg xylazine and 22 mg/kg ketamine, then a bolus intravitreal injection of 50 µL was administered to each eye at 2.5 µg/eye. Blood samples were collected at 15 and 30 minutes and 1, 2, 3, 6, 12, 24 and 48 hours. Blood samples were treated as described above. Aqueous humor samples were collected at 15 and 30 minutes and, 1, 2, 3, 6, 12, 24, 48, and 72 hours. After rabbits were euthanized, four eyeballs from two animals were collected through the use of staggered sampling. Vitreous humor samples were collected from the isolated eyeballs and weighed. The plasma, aqueous humor, and vitreous humor samples were stored at -80ºC before analysis.

Intravitreal Administration of GNE-947 in Suspension Formulation. The ocular pharmacokinetics of GNE-947 were evaluated following intravitreal administration in male Dutch-Belted rabbits with average of body weight of 2 kg. The vehicle used for the intravitreal suspension formulation was sodium carboxymethylcellulose. After the rabbits were

anesthetized as described above, intravitreal administration of 33.5 µg/eye, 100 µg/eye, 200 µg/eye at 50 µL/eye were conducted. Blood samples were collected at 15 and 30 minutes and, 1, 2, 4, 6 hours and, 1, 2, 4, 8, 15, 21, 30, 45 (for all doses), 60, 73, 92 (for 100 µg/eye and 200 µg/eye), 105 and 162 (for 200 µg/eye) days. Blood samples were treated as described above. Aqueous humor samples were collected at 6 hours, 1, 2, 4, 8, 15, and 45 days for 33.5 µg/eye; 6 hours, 1, 2, 4, 15, 45, 73, and 92 days for 100 µg/eye; 6 hours, 1, 4, 15, 45, 73, 92, and 162 days for 200 µg/eye. After the rabbits were euthanized, their eyeballs were isolated at 1, 4, 8, 15, and 45 days for 33.5 µg/eye; 1, 4, 15, 73, and 92 days for 100 µg/eye; 1, 8, 15, 73, 92, and 162 days for 200 µg/eye. The plasma, aqueous humor, and eyeball samples were stored at -80^{o}C before analysis.

MALDI-IMS Study. As described above, intravitreal injection of GNE-947 at 1 mg/eye in suspension was conducted in Dutch-Belted rabbits. The eyeballs were collected 30 days after the injection and stored at -80^{o}C before analysis. Tissue sections of eyeballs at 12 µm thickness were prepared using a cryostat (CM 3050 S, Leica Biosystems, Buffalo Grove Illinois) at -20^{o}C. Tissues were spray coated with 20 mg/mL α-cyano-4-hydroxycinnamic acid (CHCA) with a 2 µM internal standard. Tissues were analyzed on a MALDI QSTAR-QqTOF MS (AB SCIEX, Foster City, California) at m/z 454 → 397 transition at 50 µm lateral resolution. Images were processed using MALDI server 5.1.

Autoradioluminography Study. Male Dutch-Belted rabbits were administered a single intravitreal injection of ^{14}C-GNE-947 at a dose of 150 µg/20 µCi/eye in suspension as described before into each eye. After animals were euthanized at 1, 15, 30, and 60 days, their heads were sectioned at 40 µm thick using a Leica CM3600 cryomicrotome and analyzed by quantitative autoradioluminography.

LC-MS/MS Analysis. Sample analysis was carried out with a Shimadzu Nexera HPLC (Columbia, MD) coupled to a Sciex API 5500 mass spectrometer (Foster City, CA) equipped

with a turbo-electrospray interface in the positive ionization mode. The aqueous mobile phase was water with 10 mM ammonium formate (A) and the organic mobile phase was methanol (B). The gradient was 40% B between 0 and 0.4 minutes, then linearly increased to 85% B between 0.4 and 1.0 minutes, further increased to 90%B between 1.0 and 1.1 minutes, maintained at 90% between 1.1 to 1.7 minutes, decreased to 40% B between 1.7 and 2.1 minutes, and maintained at 40% B between 2.1 and 2.8 minutes. The flow rate was 1.25 mL/min and the cycle time (injection to injection including instrument delays) was approximately 3.6 minutes. A volume of 25 µL of the final extract was injected onto the analytical Agilent Zorbax SB-C18 column (50 × 2.1 mm, 5 µm).

Quantitation of GNE-947 was carried out using the multiple reaction monitoring (MRM) transition m/z 454.2 → 367.1 for GNE-947 and m/z 458.2 → 401.1 for internal standard $^{13}C^{15}N_3$-GNE-947. The choice of product ion m/z 367.1 over m/z 397.1 for GNE-947 MRM is to avoid the interference from the sample matrix while not sacrificing much signal. The signal intensity for MRM m/z 454 → 367 is about 70% of that for MRM m/z 454 → 397 transition. The optimized instrument conditions included a source temperature of 600°C, a curtain gas pressure of 15 psi, a nebulizing gas (GS1) pressure of 60 psi, a heating gas (GS2) pressure of 60 psi, and a collision energy (CE) of 45 V for both GNE-947 and $^{13}C^{15}N_3$-GNE-947. IonSpray needle voltage was set at 4000 V. LC-MS/MS data were acquired and processed using Analyst software (v1.5.2). The calibration curve for quantitation of GNE-947 was constructed by plotting the analyte (GNE-947) to internal standard ($^{13}C^{15}N_3$-GNE-947) peak area ratios versus the nominal concentration of the analyte with a weighted 1/x2 linear regression.

Aliquots of 150 µL of plasma samples, standards and quality controls were transferred to wells in the 96-well plate. Twenty five µL of internal standard (2.25 ng/mL) was added to each sample followed by the addition of 25 µL of 5% ammonium hydroxide. The samples were vortexed for 1 min and centrifuged at 1600 xg for 2 min to force all droplets to the bottom of the

wells. The entire sample was loaded to a SLE+ plate. The analytes were eluted by 2x600 µL of MTBE to a 96-well Axygen round bottom plate. The eluent was evaporated to dryness with nitrogen at 40°C and reconstituted with 80 µL of methanol:water (40:60; v:v) solution. The whole plate was vortexed and centrifuged again. Ten µL aqueous humor or vitreous humor was mixed with 25 µL of internal standard and 35 µL of methanol:water (40:60; v:v) solution. The eyeballs were cut into species with scissors and homogenized with glass beater homogenizer. Twenty µL of homogenate was mixed with 25 µL of internal standard and 1000 µL of methanol:water solution. The mixture was vortexed and centrifuged. Then 25 µL of supernatant was injected into the LC-MS/MS system for sample analysis. The lower and upper limits of quantitation of the assay were 5 and 2500 pg/mL, respectively.

Data Analysis. Noncompartmental pharmacokinetic analyses were conducted using Phoenix® WinNonlin® v6.3 (Pharsight Corporation; Mountain View, CA). Nominal doses and sampling times were used. Concentration values below the LLOQ at the end of the profile were ignored for pharmacokinetic analysis.

Compartmental pharmacokinetic analyses were constructed using SAAM II v2.3.1.1 (The Epsilon Group, Charlottesville, VA). All parameters were estimated by fitting the pharmacokinetic models to the average of the observed data at each time point. Estimates of all parameters are presented as the parameter estimate and the percent standard error.

Model for IV bolus injection. A two-compartment model (Figure 3A) was used to model GNE-947 plasma concentrations following IV administration as described by mass balance Equations 1 and 2.

$$V_c dC_c/dt = -(Cl_d+Cl_p)C_c+Cl_dC_t \qquad \text{Equation 1}$$

$$V_t dC_t/dt = Cl_d(C_c-C_t) \qquad \text{Equation 2}$$

where C_c and C_t are the concentrations of GNE-947 in the central and peripheral compartments, respectively; V_c and V_t are the volume of distribution in the central and peripheral compartments, respectively; Cl_p and Cl_d are the elimination clearance from the central compartment and distribution clearance between the compartments, respectively.

Model for the intravitreal injection of the solution formulation. A five-compartment model in Figure 4A was used to fit the drug concentrations in the plasma, vitreous humor, and aqueous humor following intravitreal injection of the solution formulation. The drug in vitreous humor was described by a vitreous humor compartment (VH Cmpt) and a binding compartment (Binding Cmpt) as described by Equations 3 and 4:

$$V_{vh}dC_{vh}/dt = -(Cl_{vp}+Cl_{va}+Cl_{vb})C_{vh}+K*A_{binding} \quad \text{Equation 3}$$

$$dA_{binding}/dt = Cl_{vb}C_{vh}-K*A_{binding} \quad \text{Equation 4}$$

where V_{vh} is the volume of distribution for the vitreous humor compartment; C_{vh} and $A_{binding}$ are the concentrations in vitreous humor and amount in the binding compartment, respectively; Cl_{vp}, Cl_{va}, and Cl_{vb} are the clearance from the vitreous humor to plasma, aqueous humor, and binding compartment, respectively; K is the rate constant form the binding compartment to vitreous humor compartment.

The drug in aqueous humor compartment (AH Cmpt) was described by Equation 5:

$$V_{ah}dC_{ah}/dt = Cl_{va}C_{vh}-Cl_{ah}*C_{ah} \quad \text{Equation 5}$$

where V_{ah} is the volume of the aqueous humor compartment which was set as the physiological volume of 0.3 mL/eye for rabbits (Del Amo 2015b); C_{ah} is the concentration in the aqueous humor; Cl_{ah} is the clearance from the aqueous humor to plasma which was set as the physiological turnover rate of 0.18 mL/hr/eye for rabbits (Del Amo 2015b).

The drug in systemic central compartment was modeled by equations 6:

$$V_c dC_c/dt=-(Cl_d+Cl_p)C_c+Cl_dC_t+2(Cl_{vp}C_{vh}+Cl_{ah}C_{ah}) \quad \text{Equation 6}$$

The drug in the systemic peripheral compartment was described same as Equation 2. Since systemic clearance and volume of distribution are determined by the physicochemical properties of the compound and the physiological system, same systemic model structure, clearance and volume of distribution parameters were used for the IV and intravitreal administration of different formulations.

Modeling for the intravitreal injection of suspension formulation. After intravitreal injection of GNE-947 in suspension formulation, the plasma concentrations showed a biphasic curve with similar maximal concentration at the three dose levels (Suppl. Figure 4) but dose proportional concentrations at later time points. We hypothesized that the 50 µL suspension formulation of GNE-947 split into two pools after intravitreal injection. The fast release pool was composed of solubilized drug at the three dose levels, resulting in similar maximal concentration in the plasma. The slow release pool compartment was composed of undissolved drug particles. It was assumed that the dose was split into a fast release pool and a slow release pool after injection as described by Equations 7-9:

For 33.5 ug/eye dose level: $Dose_{slow}= 33.5- Dose_{fast}$ Equation 7

For 100 ug/eye dose level: $Dose_{slow} = 100- Dose_{fast}$ Equation 8

For 200 ug/eye dose level: $Dose_{slow}= 200- Dose_{fast}$ Equation 9

where $Dose_{fast}$ and $Dose_{slow}$ are the doses for the fast pool and slow pool, respectively; $Dose_{fast}$ was a constant and estimated from the observed data using Split Input Function in SAAMII program.

The amount of drug in the fast and slow pools were described by Equations 10 and 11:

$$dA_{fast}/dt=-(K_1+K_2)A_{fast}+K_3(A_{slow})^{2/3} \quad \text{Equation 10}$$

$$dA_{slow}/dt=-K_3(A_{slow})^{2/3} \quad \text{Equation 11}$$

Where K_1 and K_2 are the rate constants from the fast compartment to the systemic central compartment and aqueous humor compartment, respectively; K_3 is the rate constant from the slow pool to the fast pool (Figure 5A). The rationale for selection of 2/3 exponent for the slow pool mass will be discussed in detail in the Discussion section.

The drug in aqueous humor compartment was described by equation 12:

$$V_{ah}dC_{ah}/dt= K_2A_{fast}-Cl_{ah}*C_{ah} \quad \text{Equation 12}$$

The drug in the plasma central compartment is described by Equation 13:

$$V_cdC_c/dt=-(Cl_d+Cl_p)C_c+Cl_dC_t +2(K_1A_{fast}+Cl_{ah}*C_{ah}) \quad \text{Equation 13}$$

The drug in the systemic peripheral compartment is described same as Equation 2.

In Vivo Laser Induced Choroidal Neovascular (CNV) Model. Rats were anaesthetized by i.p. injection of a mixture of ketamine and xylazine. Pupils were dilated using a single drop of 1% tropicamide. Animals were placed on a platform. Six burns of 100 micron at 532 nm diode laser photocoagulation with 120mW power for 100msec duration were delivered to the retina of the right eye using the slit lamp delivery system of an OcuLight GL Photocoagulator (Iridex, Mountain View, CA) and a hand held cover slide as a contact lens. Burns were performed 1-2 disc diameters from the optic nerve in 2, 4, 6, 8, 10 and 12 o'clock positions. Production of a bubble on the retina at the time of laser, which indicated rupture of Bruch's membrane, was an important factor in obtaining CNV, so only burns in which a bubble produced were included in

the study. Animal with burns that resulting sub-retinal hemorrhage were excluded from the study.

All animals undergoing CNV procedure were administered buprenorphine as an analgesic, SC every 8-12 hours for 2 days following laser treatment. Each dose of GND-947 were was given prior to recovery from anesthesia.

Under anesthesia, BETADINE 5% Sterile Ophthalmic Prep Solution (Alcon Laboratories, Inc.) for the eye were used to apply antiseptic to the surface area around and onto the eye 5 minutes before the injection. A 0.5 mm tip tungsten pin (Fine Science Tools 10130-20) was used to create an opening at the posterior limbus. Care was used to avoid damage to the lens. A 30 gauge Hamilton needle and syringe were used to deliver 5 µL of 50 µg or 100 µg GNE-947 in solution formulation or vehicle only through the resulted entrance site. The single maximum volume of each single intravitreal injection volume for each rat would not exceed 5 µL. Four doses of vehicle or GNE-947 were given on days 0, 3, 7 and 10 after laser injury. A postoperative application of povidone-iodine solution was given to ensure that the eye was properly disinfected after injection. All the instruments and solution used in this procedure were either sterile or sterilized and aseptic techniques were used in the injection procedure. 0.01-0.05 mg/kg buprenorphine was given to the animals for two days following the injection. Neomycin and polymyxin B sulfate and bacitracin zinc ophthalmic ointment were applied to the injected eye post injection.

Animal health status was monitored twice daily, and body weights were measured daily for the first 3 days of dosing, and twice per week if no body weight loss was observed after. The animals were weighed daily if 15% body weight loss is observed and sacrificed if 20% body weight loss is observed.

Fourteen days after laser injury, animals were injected with 1 mL of 25 mg/mL Fluorescein Dextran (Sigma, FD2000S) through tail vein injection. Five minutes after the tail vein injection, the animal was euthanized by CO_2 inhalation to effect. The eyes were removed and fixed in freshly prepared 4% paraformaldehyde in PBS for 1 hour. The cornea, lens, and retina were removed and the entire choroid with eye cup was carefully dissected. Radial cuts (4-7, average 5) were performed from the edge to the equator with care not to cut the laser injury sites and the eyecup was flat mounted and observed to fluorescence microscopy.

Results

PI3K/mTOR inhibition, HUVEC cell migration inhibition, and solubility of 10 molecules. The inhibitory potency of a selection of 10 molecules against PI3Kα and mTOR was evaluated along with the potency against cell migration in a HUVEC assay. This data, along with the solubility of the 10 molecules is presented in Table 1. Of the 10 molecules, entries **4**-**10** had HUVEC migration EC_{50}'s that were greater than 100 nM and were not selected for further evaluation due to low potency. The remaining three molecules were deemed to have adequate potency in that cellular assay. While entries **1** and **2** were the most potent molecules in the HUVEC assay, they led to solubility/cell EC_{50} ratios greater than we desired (vide infra). Therefore, entry **3** (GNE-947) was selected for further evaluation.

GNE-947 extensively binds to plasma proteins and melanin. The binding of GNE-947 to rabbit plasma proteins and melanin under various concentrations is presented in Table 2. The unbound fraction of GNE-947 in rabbit plasma was about 0.040 in the concentration range of 0.01 to 10 μM. In 1 mg/mL of melanin suspension, the unbound fraction was from 0.0030 to 0.0044 in GNE-947 concentration range of 0.1 to 10 μM. These results show that GNE-947 extensively binds to plasma proteins and melanin and its binding is concentration independent at concentrations under 10 μM.

GNE-947 shows plasma terminal $t_{1/2}$ of 9.11-9.59 hours following a single IV bolus dose in rabbits. The plasma concentrations following 2.5 μg/kg or 500 μg/kg IV bolus dose are presented in Figure 3B. Use of non-compartment analysis, the estimated terminal $t_{1/2}$ from the mean data were 9.11 and 9.59 hours for 2.5 and 500 μg/kg, respectively (Table 6). The plasma concentration-time profiles after IV dosing showed a biphasic curve. Therefore, a two-compartment model showing in Figure 3A was used to fit the observed data at 2.5 and 500 μg/kg dose levels simultaneously. The model fits well for the observed data from both doses.

The estimated compartmental PK parameters are listed in Table 3. These systemic PK parameters were used as fixed values in following ocular PK modeling because systemic clearance and volume of distribution are determined by the physicochemical properties of the compound and the physiological system.

GNE-947 shows similar plasma and vitreous humor terminal $t_{1/2}$ of 14.4-16.3 hours following intravitreal injection of a solution formulation in rabbit eyes. The plasma, vitreous humor, and aqueous humor drug concentrations following a single intravitreal injection of GNE-947 at 2.5 µg/eye in a solution formulation are presented in Figure 4B. Using a non-compartment analysis, the estimated terminal $t_{1/2}$ from the mean data were 14.4, 16.3, and 23.2 hours for plasma, vitreous humor, and aqueous humor, respectively (Table 6). The concentration-time profiles in the plasma, vitreous humor and aqueous humor are similar. The estimated area under the cures (AUC) from time zero to infinity were $2.21x10^3$, $1.16x10^6$, $7.98x10^3$ hr*pg/mL, respectively. Therefore, the AUC in vitreous humor was 145-fold higher than the aqueous humor and the AUC in aqueous humor was 3.6-fold higher than the plasma.

The concentration-time profile in vitreous humor showed a biphasic curve, indicating the compound had a distribution phase followed by an elimination phase. Because the observed concentrations in the vitreous humor were 100-fold higher than the total plasma concentrations (Figure 4B) and 2500-fold higher than the free plasma concentrations due to its plasma free fraction of 0.040, the biphasic shape of the vitreous humor concentrations in Figure 4B was not believed to be due to re-distribution of the compound from systemic circulation and the effect of plasma concentrations on vitreous humor concentrations was negligible. The aqueous humor concentrations were similar to or higher than the total plasma concentrations (Figure 4B), and 25-fold higher than the free plasma concentration, therefore the effect of plasma concentration on the aqueous humor concentrations was also negligible. Based on the observed results, a model shown in Figure 4A including 2 compartments for the systemic circulation, 2

compartments for the vitreous humor, and 1 compartment for the aqueous humor was proposed to describe the observed concentrations. This model describes the observed data well (Figure 4B). The estimated pharmacokinetic parameters are listed in Table 4.

GNE-947 shows similar plasma and vitreous humor terminal $t_{1/2}$ up to six months in the vitreous humor following intravitreal injection of a suspension formulation in rabbit eyes. Following intravitreal injection of GNE-947 at 33.5, 100, or 200 µg/eye in suspension formulation in the inferior-temporal region of the eye, the test article appeared bright white and also typically appeared as a primarily focal mass. Some diffusion for a short distance were observed around the main mass of the material.

The plasma, aqueous humor concentrations, amount in the eyes following intravitreal injection of GNE-947 are presented in Figure 5. The plasma terminal $t_{1/2}$ were 705 hr (29 day), 1760 hr (74 day), and 5250 hr (219 day) at 33.5 µg/eye, 100 µg/eye, 200 µg/eye at 50 µL/eye, respectively (Table 6). The terminal $t_{1/2}$ for the amount of drug in the eyes were 1100 hr (46 day), 3440 hr (143 day), and 4600 hr (191 day) at 33.5 µg/eye, 100 µg/eye, 200 µg/eye at 50 µL/eye, respectively (Table 6). Because there was a large variability and lack of terminal phase for the aqueous humor concentrations, the $t_{1/2}$ for aqueous humor were not calculated.

The model presented in Figure 5A described the observed plasma concentrations and the amount of drug in the eye reasonably well (Figures 5B and 5C). Since one-compartment model can adequately describe the aqueous humor concentration-time profile following an intravitreal injection of solution formulation (Fig 4B, red line), one-compartment model was used for aqueous humor compartment. There was a large variability and lack of a clear terminal elimination phase for the aqueous humor drug concentrations, the model was not able to describe the observed data well but it captures the general trend of the data (Figure 5D). The estimated pharmacokinetic parameters are listed in Table 5.

MALDI-IMS show nonhomogeneous distribution of GNE-947 in vitreous humor 30 days after intravitreal injection of a suspension formulation in rabbit eyes. GNE-947 distribution in the eye tissues using MALDI-IMS technology is presented in Figure 6. The MALDI-IMS image shows that most of GNE-947 was in the vitreous humor. In the vitreous humor, the compound was not homogeneously distributed. Some areas in the vitreous humor show white color which indicates that the drug concentration was low but in other areas show dark blue or black color indicates high drug concentrations. Low drug concentration was associated with the surface of the lens and indicated a lack of drug penetration inside the lens.

Autoradioluminographs show GNE-947 was localized at the injection site in vitreous humor for 15-60 days following intravitreal injection of suspension formulation in rabbit eyes. GNE-947 distribution in the eyes using autoradioluminography is presented in Figures 7 and 8. The drug generally remained in the inferior-temporal portion of the vitreous cavity where eyes were dosed. On day 1, most of injected drug stayed at the injection sites with small amount distributed into the vitreous humor near the injection sites. Distal to the injection sites, the drug concentration was very low. GNE-947 was present on the surface of the lens but no drug was observed to penetrate inside the lens (Figures 7A and 8A). On day 15 to day 60, most of the drug in the eyes remained at the injection site with a negligible amount in the vitreous humor (Figures 7D and 8B). Interestingly, on day 15, the drug distributed inside the lens, but did not reach the center of the lens (Figure 7D); however, by day 60, the drug had penetrated to the center of the lens (Figure 8B).

Intravitreal injection of GNE-947 was efficacious in laser induced choroidal neovascular (CNV) rat eyes. After argon laser induced damage to the rat choroid, neovascularization takes place. This neovascularization models some characteristics of vascular pathology in patients with wet AMD. Immediately after laser induced damage, GNE-947 was administered by intravitreal injection at 50 or 100 µg/eye (Fig 9A) and again on days 3, 7, and 10. On day 14 of

the study, tissues were harvested and the extent of neovascularization was determined by microscopy evaluation, by measuring the area of lesion. Compared to the vehicle controls, the animals treated with either 50 or 100 µg/eye had significantly reduced lesion area (Fig 9B).

Discussion

Current anti-VEGF therapies have had a dramatic impact on wAMD treatment but require frequent intravitreal injections (4-6 weeks). In addition, only 30-40% of wet AMD patients are complete responders to anti-VEGF therapy and so a different mechanism of action may add increased efficacy to some patients (Chang et al. 2007; Bressler et al. 2009; Busbee et al. 2013; Heier et al. 2012). Thus, the unmet needs in the treatment of wet AMD are reduced dosing frequency and increased efficacy in incomplete responders. We sought a drug that would achieve long duration of treatment for wet AMD patients by inhibiting PI3K/mTOR pathways.

At the onset of this program, we had ready access to many potent PI3K and PI3K/mTOR inhibitors (Folkes 2008; Heffron 2011; Ndubaku 2013; Staben 2010; Staben 2011; Staben 2013a; Staben 2013b; Sutherlin 2010; Sutherlin 2011). Unique to this program for the treatment of retinal diseases, we wanted to ensure that the solubility was high enough to ensure the ability to sustain concentrations in the vitreous humor (to allow access to retina) 10-fold over the cellular EC_{50}. As we sought a long lasting depot of drug in suspension, however, we also wanted the solubility of the molecules to be not too high to render short duration for the depot effects. For this reason, our target profile of PI3K/mTOR inhibitor was one that had a ratio of the solubility of the molecule to cellular EC_{50} that was in the 20-50 fold range. While we had previously identified PI3K inhibitors that had advanced to clinical trials for cancer treatment, we deemed these molecules inadequate for this use as they had solubility/cell EC_{50} ratios that exceeded our target range (Suppl. Figure 1). As our previous development candidates did not meet our target criteria with respect to solubility/cellular EC_{50}, we selected 10 additional PI3K inhibitors to evaluate in a HUVEC migration assay and determined the kinetic solubility of these same molecules at pH 7.2 (Table 1). These molecules were selected from multiple chemical scaffolds (Suppl. Figure 2). GNE-947 met our criteria for further study and additional data is presented in Suppl Figure 3.

In the present study, we showed that GNE-947 has a biphasic PK profile with terminal $t_{1/2}$ of less than a day after a single intravitreal injection in a solution in rabbit eyes, which is slightly longer than the IV dose. Interestingly, it has a terminal $t_{1/2}$ of up to six months after a single intravitreal injection in a suspension at higher doses. These results support the feasibility to design a PI3K/mTOR inhibitor to treat wet AMD using intravitreal injection with dosing frequency of potentially once a year. The learning from GNE-947 ocular PK studies is helpful in designing drugs for the treatment of wet AMD and other posterior eye diseases that require a long duration of exposure.

Many ocular PK studies utilizing intravitreal administration are reported in the literature. However, few studies examined the drug concentrations in plasma, vitreous humor, and aqueous humor simultaneously, which is apparently due to a lack of sensitive bioanalytical methods to determine low drug concentration in the plasma (Urtti, 2006, del Amo et, 2015b). In the present study, we developed a sensitive mass spectrometry method that was able to detect 5 pg/mL (11 pM) as the lower limit of quantitation. This method allowed us to monitor the plasma concentrations following dosing as low as 2.5 µg/eye in a solution formulation or monitor the plasma concentrations for several months following dosing of 200 µg/eye in a suspension formulation. The extensive data generated in this study will be helpful to develop ocular PBPK and ocular in silico $t_{1/2}$ prediction models to enable the design of drugs for the treatment of retinal diseases (Kidron et al, 2012; del Amo et al, 2015a, del Amo et, 2015b, Vellonen et al, 2016, Durairaj et al, 2008).

After intravitreal injection of GNE-947 in solution formulation, the concentration-time profiles in vitreous humor, aqueous humor and plasma were biphasic and parallel. A two-compartment model with a vitreous humor compartment and a hypothetical binding compartment were proposed based on the observed biphasic profiles and high binding affinity to melanin. The estimated terminal $t_{1/2}$ from the mean vitreous humor was 16.3 hours. This value is consistent

with the range of reported intravitreal $t_{1/2}$ of 0.62-26.5 hours (del Amo et al, 2015a). The estimated transfer clearance from vitreous humor to plasma (Clvp) was 0.408 mL/hr/eye. This value is consistent with the range of reported intravitreal clearance of 0.031-1.53 mL/hr/eye (del Amo et al, 2015a). The estimated volume for the vitreous compartment was 5.19 mL/eye, which is outside the range of 0.72-3.14 mL/eye reported in the literature for marketed drugs (del Amo et al, 2015a). This may be due to higher lipophilicity of GNE-947 than marketed drugs studied in the literature.

There are two elimination routes from the eye for intravitreally injected drugs: anterior elimination of the drug through the aqueous humor flow and posterior elimination through blood-ocular barriers such as iris epithelium, non-pigmented ciliary epithelium and retinal capillaries (Urtti, 2006, Ranta et al, 2006). Large, hydrophilic compounds with low membrane permeability such as antibody drugs are cleared from the vitreous humor via the anterior elimination route and lipophilic low molecular weight drugs with high permeability are cleared via the posterior elimination route. In the present study, the posterior elimination clearance is about 1000-fold higher than the anterior elimination clearance, indicating most of the GNE-947 was eliminated via a posterior route. This observation is consistent with the clearance mechanism for other low molecular weight compounds reported in the literature (Del Amo 2015b).

In suspension formulation, the plasma concentrations showed a biphasic curve with similar maximal concentration at the three dose levels (Suppl. Figure 4) but dose proportional concentrations at later time points. We hypothesized that the 50 µL suspension formulation of GNE-947 split into two pools after intravitreal injection. We propose that a fast-release pool, which was composed of solubilized drug and small size particles similar at the three dose levels, resulted in similar maximal concentration in the plasma regardless of dose levels as the injection volume was kept at 50 µL for the 3 doses. We also propose that a slow-release pool compartment was composed of large particles, which required a longer time for distribution

and/or elimination. The amount in the fast-release pool was estimated as 4.54 µg/eye, which was estimated by fitting the model to the observed plasma concentrations and the amount in the eyes, which was only a small fraction of the administered dose (33.5-200 µg/eye).

In suspension formulation, there was a trend that the $t_{1/2}$ increased with increasing dose levels for both the plasma concentration and amount of drug in the eyes. In addition, using the model shown in Figure 5A, using first-order transfer (K3) from the slow release compartment to the fast release compartment, described the observed plasma concentration well for the middle dose but it slightly over-predicted the plasma concentrations for the high dose and slightly under-predicted it for the low dose (Suppl. Figure 5). To explain the observed data, we assumed that the release rate from the slow release pool to the fast release pool was determined by the dissolution rate as expressed by the Noyes–Whitney equation or the Nernst and Brunner equation (Dokoumetzidis and Macheras, 2006):

$$\text{Dissolution rate} = A*D*(C_s-C_b)/d \qquad \text{Equation 14}$$

where *A* is surface area of the particles, D is diffusion coefficient, C_s is solubility, C_b is the concentration in the vitreous humor, d is thickness of the boundary layer of the solvent at the surface of the dissolving substance.

If we assume the particles are spheres, the relationship between the surface area (A) and mass of the drug is (Kim et al, 2006):

$$A = (6\sqrt{\pi}\, Mass/density)^{2/3} \qquad \text{Equation 15}$$

From Equations 14 and 15, we derived that dissolution rate is proportional to the $Mass^{2/3}$ and used this relationship in Equations 10 and 11 for the model in Figure 5A. This model improved the prediction for the high dose and the low dose based on a visual inspection.

The results from our MALDI-IMS imaging and autoradioluminography studies were consistent with the assumption that dissolution was the rate-limiting step for the clearance of the drug in the vitreous humor. The MALDI-IMS image shows that most of GNE-947 was in the vitreous humor and was not homogeneously distributed on day 30. The autoradioluminography studies clearly showed that drug in the vitreous humor remained as a single aggregate form, which resulted in reduced surface area exposed to the vitreous humor. This may have led to further decreasing its dissolution rate in addition to its low solubility.

In a CNV efficacy study (Figure 9), a significant effect was demonstrated at both doses tested. For infrequent drug administration we think there may be an optimal range for the solubility of a drug such that the solubility is low enough to allow long duration but the rate of dissolution must be sufficiently high to maintain a sufficient concentration to inhibit its targets.

The plasma $t_{1/2}$ following an intravitreal injection is mainly determined by the slowest step of following kinetic processes: release of the drug from its formulation, ocular distribution, transfer from ocular tissue to systemic circulation, and finally systemic distribution and elimination. The plasma $t_{1/2}$ of 14.4-16.3 hours following an intravitreal injection of a low dose solution was slightly longer than 9.11-9.59 hours following an IV administration, indicating ocular distribution and/or transfer from ocular tissue to systemic circulation is slightly slower than the systemic distribution and elimination for this drug. Interestingly, the observed plasma $t_{1/2}$ of 6 months following an intravitreal injection of a high dose suspension was much longer than that of an intravitreal injection of a low dose solution or an IV administration, indicating the release of drug from its suspension formulation is the slowest step and determines to the observed long plasma $t_{1/2}$. Our PK modeling, MALDI-IMS imaging, and autoradioluminography results consistently support this explanation.

In summary, the present work shows GNE-947 is a potent PI3K/mTOR inhibitor and exhibits anti-CNV activity in rat eyes. The duration of GNE-947 in the rabbit eyes following intravitreal injection in a solution is short with $t_{1/2}$ less than a day. However, the duration following intravitreal dose of a suspension is very long with $t_{1/2}$ up to six months due to its low solubility and slow dissolution process. These results indicate that intravitreal injection of a suspension formulation for low solubility drugs can be used to achieve long-term drug exposure potentially useful for the treatment of wet AMD and other retinal diseases.

Acknowledgements

The authors thank Jialin Mao and QPS for their assistance for the plasma protein binding and melanin binding study, Weilan Ye and Vladimir Bansteev for help in preparation of the manuscript and Jason Ho, Cynthia Young, Kirsten Messeck for conducting in vivo study.

Authorship Contributions

Participated in research design: Liu, Heffron, Liang, Wright, Hop, LeCouter, Lubach, Shahidi-Latham

Conducted experiments: Liang, Ubhayakar, Chen, Cheng, Lee, Quiason, LeCouter, Lubach, Solon

Contributed new reagents or analytical tools: Heffron

Performed data analysis: Liu, Chen

Wrote or contributed to the writing of the manuscript: Liu, Heffron, Liang, Ye

References

Bressler NM, Chang TS, Fine TJ, Dolan CM and Ward J (2009) Improved vision-related function after ranibizumab vs photodynamic therapy: a randomized clinical trial. *Arch Ophthalmol* 127:13−21.

Busbee BG, Ho AC, Brown DM, Heier JS, Suner IJ, Li Z, Rubio RG and Lai P (2013) Twelve-month efficacy and safety of 0.5 mg or 2.0 mg ranibizumab in patients with subfoveal neovascular age-related macular degeneration. *Ophthalmol* 120:1046−1056.

Caballero S, Swaney J, Moreno K, Afzal A, Kielczewski J, Stoller G, Cavalli A, Garland W, Hansen G, Sabbadini R and Grant MB (2009) Anti-sphingosine-1-phosphate monoclonal antibodies inhibit angiogenesis and sub-retinal fibrosis in a murine model of laser-induced choroidal neovascularization. *Exp Eye Res* 88:367−377.

Chang TS, Bressler NM, Fine JT, Dolan CM, Ward J and Klesert TR (2007) Improved vision-related function after ranibizumab treatment of neovascular age-related macular degeneration: results of a randomized clinical trial. *Arch Ophthalmol* 125:1460−1469.

del Amo 2015a: del Amo EM, Vellonen K, Kidron H and Urtti A (2015) Intravitreal clearance and volume of distribution of compounds in rabbits: in silico predition and PK simulations for drug development. *Euro J Pharm Biopharm* 95(Pt B):215-226.

del Amo 2015b: del Amo EM and Urtti A (2015) Rabbit as an animal model for intravitreal pharmacokinetics: clinical predictability and quality of the published data. *Exp Eye Res* 137:111-124.

Dokoumetzidis A and Macheras P (2006) A century of dissolution research: From Noyes and Whitney to the Biopharmaceutics Classification System. *Int J Pharm* 321:1–11.

Durairaj C, Shan JC, Senapati S and Kompella UB (2009) Prediction of vitreal half-life based on drug physicochemical properties: Quantitative structure-pharmacokinetic relationships (QSPKR). *Pharm Res* 26:1236-1260.

Ferrara N (1999) Molecular and biological properties of vascular endothelial growth factor. *J Mol Med* 77:527−543.

Ferrara N, Gerber HP and LeCouter J (2003) The biology of VEGF and its receptors. *Nat Med* 9:669−676.

Ferrara N, Damico L, Shams N, Lowman H and Kim R (2006) Development of ranibizumab, an anti-vascular endothelial growth factor antigen binding fragment, as therapy for neovascular age-related macular degeneration. *Retina* 26:859−870.

Folkes AJ, Ahmadi K, Alderton WK, Alix S, Baker SJ, Box G, Chuckowree IS, Clarke PA, Depledge P, Eccles SA, Friedman LS, Hayes A, Hancox TC, Kugendradas A, Lensun L, Moore P, Olivero AG, Pang J, Patel S, Pergl-Wilson GH, Raynaud FI, Robson A, Saghir N, Salphati L, Sohal S, Ultsch MH, Valenti M, Wallweber HJ, Wan NC, Wiesmann C, Workman P, Zhyvoloup A, Zvelebil MJ and Shuttleworth SJ (2008) The identification of 2-(1H-indazol-4-yl)-6-(4-methanesfulfonyl-piperazin-1-ylmethyl)-4-morpholin-4-yl-thieno[3,2-d]pyrimidine (GDC-0941) as a potent, selective, orally bioavailable inhibitor of class I PI3 kinase for the treatment of cancer. *J Med Chem* 51:5522-5532.

Gerber HP, McMurtrey A, Kowalski J, Yan M, Keyt BA, Dixit V and Ferrara N (1998) Vascular endothelial growth factor regulates endothelial cell survival through the phosphatiylinositol 3'-kinase/Akt signal transduction pathway. Requirement for Flt-1/KDR activation. *J Biol Chem* 273:30336−303343.

Gaudana R, Jwala J, Boddu SH and Mitra AK (2009) Recent perspectives in ocular drug delivery. *Pharm Res* 26:1197-1216.

Graupera M, Guillermet-Guibert J, Foukas LC, Phng LK, Cain RJ, Salpekar A, Pearce W, Meek S, Millan J, Cutillas PR, Smith AJ, Ridley AJ, Ruhrberg C, Gerhardt H and Vanhaesebroeck B (2008) Angiogenesis selectively requires the p110alpha isoform of PI3K to control endothelial cell migration. *Nature* 453:662−666.

Hamada K, Sasaki T, Koni PA, Natsui M, Kishimoto H, Sasaki J, Yajima N, Horie Y, Hasegawa G, Naito M, Miyazaki J, Suda T, Itoh H, Nakao K, Mak TW, Nakano T and Suzuki A (2005) The PTEN/PI3K pathway governs normal vascular development and tumor angiogenesis. *Genes Dev* 19:2054−2065.

Heffron TP, Wei B, Olivero A, Staben ST, Tsui V, Do S, Dotson J, Folkes AJ, Goldsmith P, Goldsmith R, Gunzner J, Lesnick J, Lewis C, Mathieu S, Nonomiya J, Shuttleworth S, Sutherlin DP, Wan NC, Wang S, Wiesmann C and Zhu BY (2011) The rational design of PI3 kinase inhibitors exhibiting selectivity over the PI3K-β isoform. *J Med Chem* 54:7815-7833.

HeffronTP, Heald, RA, Ndubaku C, Wei B, Augistin M, Do S, Edgar K, Eigenbrot C, Friedman L, Gancia E, Jackson PS, Jones G, Kolesnikov A, Lee LB, Lesnick JD, Lewis C, McLean N, Mortl M, Nonomiya J, Pang J, Price S, Prior WW, Salphati L, Sideris S, Staben ST, Steinbacher S, Tsui V, Wallin J, Sampath D, Olivero AG The rational design of selective benzoxazepin inhibitors of the α-isoform of phosphoinositide 3-kinase culminating in the identification of (*S*)-2-((2-(1-Isopropyl-1*H*-1,2,4-triazol-5-yl)-5,6-dihydrobenzo[*f*]imidazo[1,2-*d*][1,4]oxazepin-9-yl)oxy)propanamide (GDC-0326). *J Med Chem* 59, 985-1002.

Heffron TP, Salphati L, Alicke B, Cheong J, Dotson J, Edgar K, Goldsmith R, Gould SE, Lee LB, Lesnick JD, Lewis C, Ndubaku C, Nonomiya J, Olivero AG, Pang J, Plise EG, Sideris S, Trapp

S, Wallin J, Wang L, Zhang X The design and identification of brain penetrant inhibitors of phosphoinositide 3-kinase α. *J Med Chem*, 55, 8007-8020.

Heier JS, Brown DM, Chong V, Korobelnik JF, Kaiser PK, Nguyen QD, Kirchhof B, Ho A, Ogura Y, Yancopoulos GD, Stahl N, Vitti R, Berliner AJ, Soo Y, Anderesi M, Groetzbach G, Sommerauer B, Sandbrink R, Simader C and Schmidt-Erfurth U (2012) Intravitreal aflibercept (VEGF trap-eye) in wet age-related macular degeneration. *Ophthalmol* 119:2537−2548.

Jo N, Mailhos C, Ju M, Cheung E, Bradley J, Nishijima K, Robinson GS, Adamis AP and Shima DT (2006) Inhibition of platelet-derived growth factor B signaling enhances the efficacy of anti-vascular endothelial growth factor therapy in multiple models of ocular neovascularization. *Am J Pathol* 168:2036−2053.

Kidron H, del Amo EM, Vellonen KS and Urtti A (2012) Prediction of the vitreal hal-life of small molecular drug-like compounds. *Pharm Res* 29:3302-3311.

Kim H, Csaky KG, Chan CC, Bungay PM, Lutz RJ, Dedrick RL, Yuan P, Rosenberg J, Grillo-Lopez AJ, Wilson WH and Robinson MR (2006) The pharmacokinetics of rituximab following an intravitreal injection. *Exp Eye Res* 82:760-766.

Koeberle MJ, Hughes PM, Skellern GG and Wilson CG (2003) Binding of memantine to melanin: influence of type of melanin and characteristics. *Pharm Res* 20:1702-1709.

Lin B and Pease JH (2016) A high throughput solubility assay for drug discovery using microscale shake-flask and rapid UHPLC-UV-CLND quantification. *J Pharm Biomed Anal* 122:126-140.

Miller JW, Le Couter J, Strauss EC and Ferrara N (2013) Vascular endothelial growth factor A in intraocular vascular disease. *Ophthalmol* 120:106−114.

Ndubaku CO, Heffron TP, Staben ST, Baumgardner M, Blaquiere N, Bradley E, Bull R, Do S, Dotson J, Dudley D, Edgar KA, Friedman LS, Goldsmith R, Heald RA, Kolesnikov A, Lee L, Lewis C, Nannini M, Nonomiya J, Pang J, Price S, Prior WW, Salphati L, Sideris S, Wallin JJ, Wang L, Wei B, Sampath D and Olivero AG (2013) Discovery of 2-{3-[2-(1-Isopropyl-3-methyl-1*H*-1,2–4-triazol-5-yl)-5,6-dihydrobenzo[f]imidazo[1,2-*d*][1,4]oxazepin-9-yl]-1*H*-pyrazol-1-yl}-2-methylpropanamide (GDC-0032): A β-sparing phosphoinositide 3-kinase inhibitor with high unbound exposure and robust in vivo antitumor activity. *J Med Chem* 56: 4597-4610.

O'Reilly KE, Rojo F, She QB, Solit D, Mills GB, Smith D, Lane H, Hofmann F, Hicklin DJ, Ludwig DL, Baselga J and Rosen N (2006) mTOR inibition induces upstream receptor tyrosine kinase signaling and activates Akt. *Cancer Res* 66:1500−1508.

Ranta VP and Urtti A (2006) Transscleral drug delivery to the posterior eyes: Prospects of pharmacokinetic modeling. *Adv Drug Deliv Rev* 58:1164-1181.

Regillo CD, Brown DM, Abraham P, Yue H, Ianchulev T, Schneider S and Shams N (2008) Randomized, double-masked, sham-controlled trial of ranibizumab for neovascular age-related macular degeneration: PIER Study year 1. *Am J Ophthalmol* 145:239−248.

Sampath D, Oeh J, Wyatt SK, Cao TC, Koeppen H, Eastham-Anderson J, Robillard L, Ho CC, Ross J, Zhuang G, Reslan HB, Vitorino P, Barck KH, Ungersma SE, Vernes JM, Caunt M, Van Bruggen N, Ye W, Vijapurkar U, Meng YJ, Ferrara N, Friedman LS and Carano RA (2013) Multimodal microvascular imaging reveals that selective inhibition of class I PI3K is sufficient to induce an antivascular response. *Neoplasia* 15:694−711.

Schmidt-Erfurth U, Eldem B, Guymer R, Korobelnik JF, Schlingemann RO, Axer-Siegel R, Wiedemann P, Simader C, Gekkieva M and Weichselberger A (2011) Efficacy and safety of monthly versus quarterly ranibizumab treatment in neovascular age-related macular degeneration: The EXCITE study. *Ophthalmol* 118:831−839.

Schnell CR, Stauffer F, Allegrini PR, O'Reilly T, McSheehy PM, Dartois C, Stumm M, Cozens R, Littlewood-Evans A, García-Echeverría C and Maira SM (2008) Effects of the dual phosphatidylinositol 3-kinase/mammalian target of rapamycin inhibitor NVP-BEZ235 on the tumor vasculature: implications for clinical imaging. *Cancer Res* 68:6598−6607.

Staben ST, Siu M, Goldsmith R, Olivero AG, Do S, Burdick DJ, Heffron TP, Dotson J, Sutherlin DP, Zhu BY, Tsui V, Le H, Lee L, Lesnick J, Lewis C, Murray JM, Nonomiya J, Pang J, Prior WW, Salphati L, Rouge L, Sampath D, Sideris S, Wiesmann C and Wu P (2011) Structure-based design of thienobenzoxepin inhibitors of PI3-kinase. *Bioorg Med Chem Lett* 21:4054-4058.

Staben ST, Heffron TP, Sutherlin DP, Bhat SR, Castanedo GM, Chuckowree IS, Dotson J, Folkes AJ, Friedman LS, Lee L, Lesnick J, Lewis C, Murray JM, Nonomiya J, Olivero AG, Plise E, Pang J, Prior WW, Salphati L, Rouge L, Sampath D, Tsui V, Wan NC, Wang S, Weismann C, Wu P and Zhu BY (2010) Structure-based optimization of pyrazolo–pyrimidine and –pyridine inhibitors of PI3 kinase. *Bioorg Med Chem Lett* 20:6048-6051.

Staben 2013a: Staben ST, Ndubaku C, Blaquiere N, Belvin M, Bull RJ, Dudley D, Edgar K, Gray D, Heald R, Heffron TP, Jones GE, Jones M, Kolesnikov A, Lee L, Lesnick J, Lewis C, Murray J, McLean NJ, Nonomiya J, Olivero AG, Ord R, Pang J, Price S, Prior WW, Rouge L, Salphati L, Sampath D, Wallin J, Wang L, Wei B, Weismann C and Wu P (2013) Discovery of thiazolobenzoxepin PI3-kinase inhibitors that spare the PI3-kinase β isoform. *Bioorg Med Chem Lett* 23:2606-2613.

Staben 2013b: Staben ST, Blaquiere N, Tsui V, Kolesnikov A, Do S, Bradley EK, Dotson J, Goldsmith R, Heffron TP, Lesnick J, Lewis C, Murray J, Nonomiya J, Olivero AG, Pang J, Rouge L, Salphati L, Wei B, Wiesmann C and Wu P (2013) Cis-amide isosteric replacement in thienobenzoxepin inhibitors of PI3-kinase. *Bioorg Med Chem Lett* 23:897-901.

Sutherlin DP, Sampath D, Berry M, Castanedo G, Chang Z, Chuckowree I, Dotson J, Folkes A, Friedman L, Goldsmith R, Heffron T, Lee L, Lesnick J, Lewis C, Mathieu S, Nonomiya J, Olivero A, Pang J, Prior WW, Salphati L, Sideris S, Tian Q, Tsui V, Wan NC, Wang S, Wiesmann C, Wong S and Zhu BY (2010) Discovery of (thienopyrimidin-2-yl)aminopyrimidines as potent, selective, and orally available pan-PI3-kinase and dual pan-PI3-kinase/mTOR inhibitors for the treatment of cancer. *J Med Chem* 53:1086-1097.

Sutherlin DP, Bao L, Berry M, Castanedo G, Chuckowree I, Dotson J, Folks A, Friedman L, Goldsmith R, Gunzner J, Heffron T, Lesnick J, Lewis C, Mathieu S, Murray J, Nonomiya J, Pang J, Pegg N, Prior WW, Rouge L, Salphati L, Sampath D, Tian Q, Tsui V, Wan NC, Wang S, Wei B, Wiesmann C, Wu P, Zhu BY and Olivero A (2011) Discovery of a potent, selective, and orally available Class I phosphatidylinositol 3-kinase (PI3K)/mammalian target of rapamycin (mTOR) kinase inhibitor (GDC-0980) for the treatment of cancer. *J Med Chem* 54:7579-7587.

Urtti A (2006) Challenges and obstacles of ocular pharmacokinetics and drug delivery. *Adv Drug Deliv Rev* 58:1131-1135.

Vellone KS, Soini EM, del Amo EM and Urtti A (2016) Molecular Pharmaceutics, Prediction of ocular drug distribution from systemic blood circulation. *Mol Pharm* 13:2906-2911.

Wallin JJ, Guan J, Prior WW, Lee LB, Berry L, Belmont LD, Koeppen H, Belvin M, Friedman LS and Sampath D (2012) GDC-0941, a novel class I selective PI3K inhibitor, enhances the efficacy of docetaxel in human breast cancer models by increasing cell death in vitro and in vivo. *Clin Cancer Res* 18:3901−11.

Yuan TL, Choi HS, Matsui A, Benes C, Lifshits E, Luo J, Frangioni JV and Cantley LC (2008) Class 1A PI3K regulates vessel integrity during development and tumorigenesis. *Proc Natl Acad Sci USA* 105:9739−44.

Figure Legends

Figure 1. GNE-947 targets PI3K and mTOR kinases to inhibit endothelial cell survival, migration, and vascular permeability induced by VEGF.

Figure 2. Structures of GNE-947, its stable isotope labeled form, and radioactive isotope labeled form. The asterisk sign shows the labeled atoms.

Figure 3. GNE-947 plasma concentration-time profiles following a single IV bolus dose of 25 µg/kg (red) or 500 µg/kg (black) in rabbits. Figure 3A is a 2-compartmental model to describe the plasma PK. The lines in Figure 3B represent the predicted concentrations from the model in Figure 3A. The PK parameters are listed in Table 3.

Figure 4. 4A is a 5-compartmental model to describe the plasma and ocular PK for the solution formulation. GNE-947 plasma (black), aqueous humor (red), and vitreous humor (blue) concentration versus time following a single intravitreal dose of 2.5 µg/eye in a solution formulation. The lines in Figure 4B represent the predicted concentrations from the model in Figure 4A. The PK parameters are listed in Table 4.

Figure 5. 5A is a 5-compartmental model to describe the plasma and ocular PK for the suspension formulation. The dash line compartment represents total amount of drug in the eyes excluding the drug in the aqueous humor. GNE-947 plasma concentrations (B), the total amount of drug in the eyes excluding drug in the aqueous humor (C), and aqueous humor concentration (D) versus time following a single intravitreal dose of 33.5 (circles), 100 (triangles), and 200 µg/kg (squares) in a suspension formulation. The lines in Figures 5B, C, and D represent the predicted concentrations from the model in Figure 5A. The PK parameters listed in Table 5.

Figure 6. Optical (A) and MALDI (B) images of a rabbit sagittal eye section following a single intravitreal dose of 1000 µg/eye of GNE-947 on day 30.

Figure 7. Optical images and autoradiographs of rabbit frontal eye sections following a single intravitreal dose of 150 µg/eye of GNE-947 on day 1 or day 15.

Figure 8. Autoradiographs of rabbit sagittal eye sections following a single intravitreal dose of 150 µg/eye of GNE-947 on day 1 or day 60.

Figure 9. Rat CNV efficacy study design and lesion location (9A), and imaging analysis (9B) after day 14 for animals dosed with GNE-947 at 50 or 100 ug per eye.

Table 1. Potency and solubility data for studied PI3K inhibitors.

Compounds	PI3Kα Ki app uM	mTOR Ki app uM	HUVEC EC_{50} uM	Solubility uM (pH 7.2)	Solubility/ HUVEC EC_{50}
1	0.0002	0.026	0.042	4.2	100
2	0.0007	0.03	0.061	26	426
3 (GNE-947)	<0.00005	0.044	0.093	2.2	24
4	0.005	0.022	0.171	12	72
5	0.006	0.75	0.184	4.7	26
6	0.0006	0.025	0.189	15	78
7	0.00009	0.21	0.203	1.1	5.4
8	0.018	0.044	0.303	12	41
9	0.006	0.059	0.882	12	14
10	0.004	0.011	>1.000	2	<2

Table 2: Free fraction of GNE-947 in rabbit plasma and melanin suspension (Mean ± SD, n=3)

Concentration (µM)	Plasma	Melanin Suspension
0.01	0.040 ± 0.000	NC
0.1	NC	0.0030 ± 0.0001
0.3	0.039 ± 0.002	0.0032 ± 0.0005
1	NC	0.0039 ± 0.0004
3	NC	0.0044 ± 0.0013
10	0.043 ± 0.005	0.0038 ± 0.0006

NC: studies were not conducted.

Table 3. GNE-947 pharmacokinetic parameters following a single IV dose at 25 or 500 µg/kg in rabbits.

Parameter	Unit	Value	CV%
Cl	mL/hr/kg	1139	3.87
Cld	mL/hr/kg	275	8.27
V1	mL/kg	2645	3.04
V2	mL/kg	6439	40.0

Table 4. GNE-947 pharmacokinetic parameters following a single intravitreal injection at 2.5 µg/eye in a solution formulation in rabbit eyes.

Parameter	Unit	Value	CV%
Cl	mL/hr/kg	1139	Fixed[a]
Cld	mL/hr/kg	275	Fixed[a]
V1	mL/kg	2645	Fixed[a]
V2	mL/kg	6439	Fixed[a]
Clah	mL/eye	0.18	Fixed[b]
Vah	mL/eye	0.3	Fixed[b]
Clvp	mL/hr/eye	0.408	6.07
Clva	mL/hr/eye	0.000398	24.7
Clvb	mL/hr/eye	0.029	28.9
K	hr^{-1}	0.0578	17.1
Vvh	mL/eye	5.19	12.4

[a]Results from IV bolus PK modeling in Figure 3

[b]Physiological value

Table 5. GNE-947 pharmacokinetic parameters following a single intravitreal injection at 33.5, 100 or 200 µg/eye in a suspension formulation in rabbit eyes.

Parameter	Unit	Value	CV%
Cl	mL/hr/kg	1139	Fixed[a]
Cld	mL/hr/kg	275	Fixed[a]
V1	mL/kg	2645	Fixed[a]
V2	mL/kg	6439	Fixed[a]
Clah	mL/eye	0.18	Fixed[b]
Vah	mL/eye	0.3	Fixed[b]
$Dose_{fast}$	ug/eye	4.54	18.8
K1	hr^{-1}	0.0150	20.0
K2	hr^{-1}	0.0000366	11.9
K3	hr^{-1}	0.122	6.17

[a]Results from IV bolus PK modeling in Figure 3

[b]Physiological value

Table 6. GNE-947 half-lives following a single IV or intravitreal injection in rabbits.

Route	Dose	Formulation	Matrix	Half-life (hr)
IV	2.5 µg/kg	Solution	Plasma	9.11
IV	500 µg/kg	Solution	Plasma	9.59
ITV	2.5 µg/eye	Solution	Plasma	14.4
			Vitreous humor	16.3
			Aqueous humor	23.2
ITV	33.5 µg/eye	Suspension	Plasma	705
			Eye	1100
ITV	100 µg/eye	Suspension	Plasma	1760
			Eye	3440
ITV	200 µg/eye	Suspension	Plasma	5250
			Eye	4600

Fig. 1

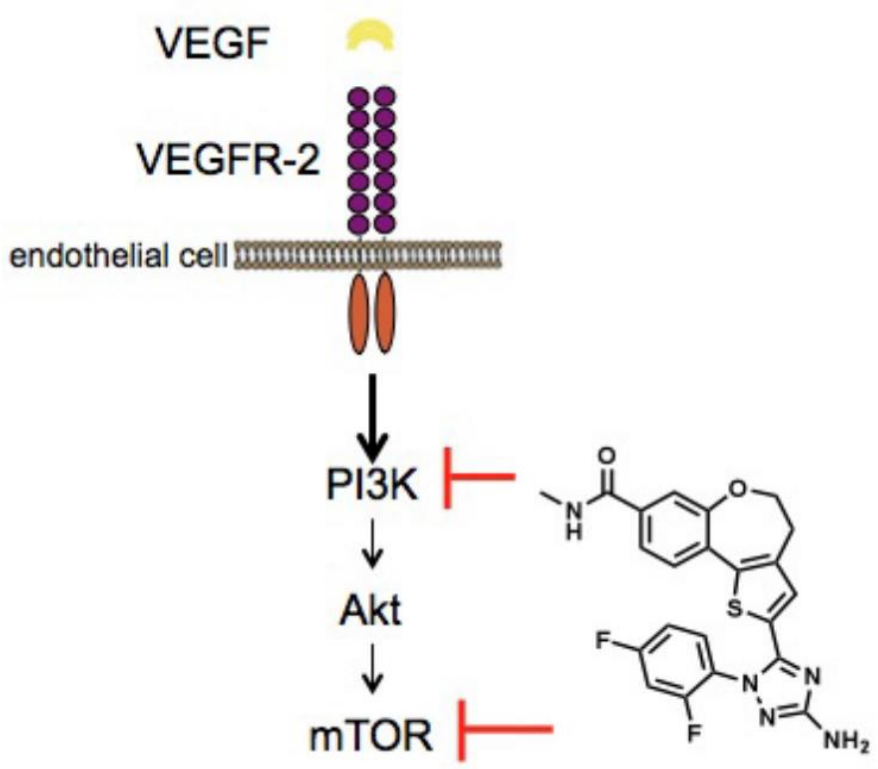

Fig. 2

GNE-947

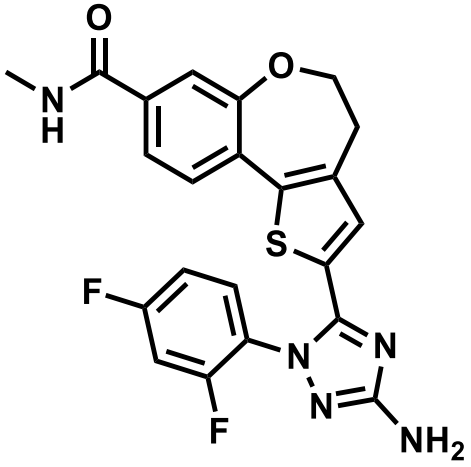

$^{13}C^{15}N_3$-GNE-947

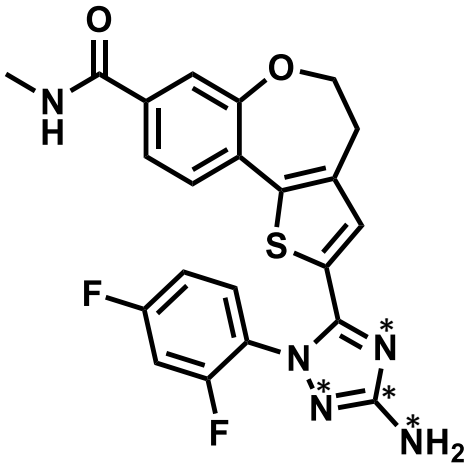

^{14}C-GNE-947

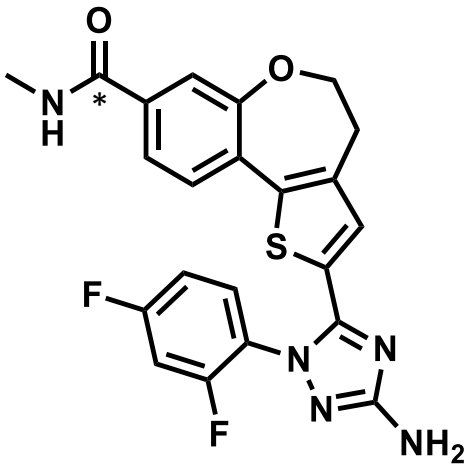

Fig. 3

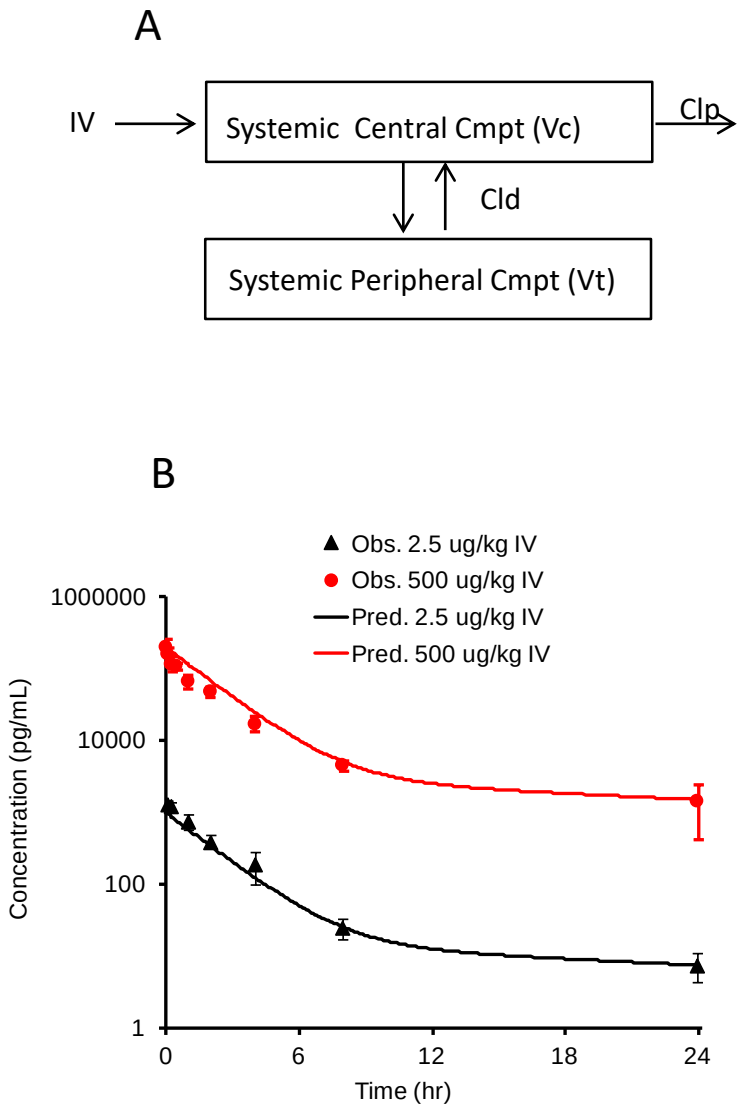
A
IV
Systemic Central Cmpt (Vc)
Clp
Cld
Systemic Peripheral Cmpt (Vt)
B
Obs. 2.5 ug/kg IV
Obs. 500 ug/kg IV
Pred. 2.5 ug/kg IV
Pred. 500 ug/kg IV
Concentration (pg/mL)
1000000
10000
100
1
0
6
12
18
24
Time (hr)

Fig. 4

A

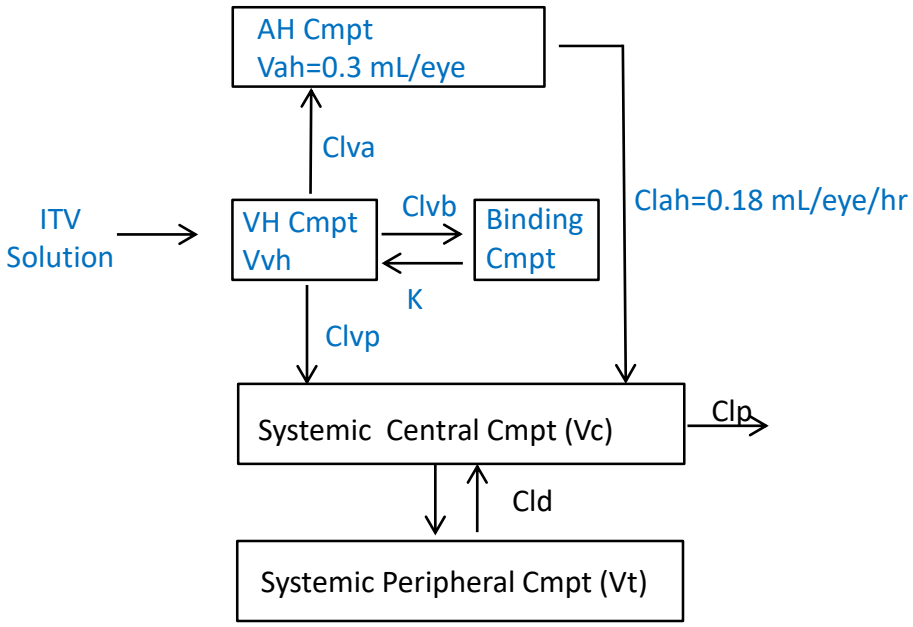
AH Cmpt
Vah=0.3 mL/eye
Clva
ITV
Solution
VH Cmpt
Vvh
Clvb
Binding
Cmpt
K
Clah=0.18 mL/eye/hr
Clvp
Systemic Central Cmpt (Vc)
Clp
Cld
Systemic Peripheral Cmpt (Vt)

B

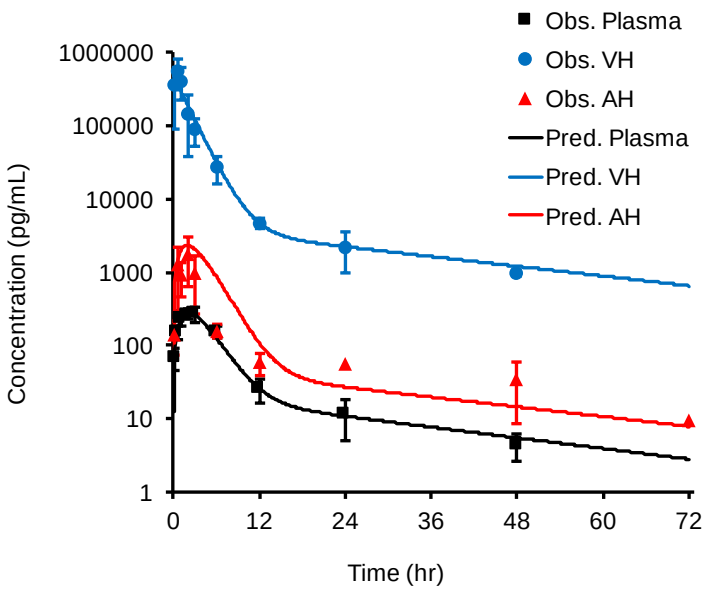
Obs. Plasma
Obs. VH
Obs. AH
Pred. Plasma
Pred. VH
Pred. AH
Concentration (pg/mL)
1000000
100000
10000
1000
100
10
1
0
12
24
36
48
60
72
Time (hr)

Fig. 5

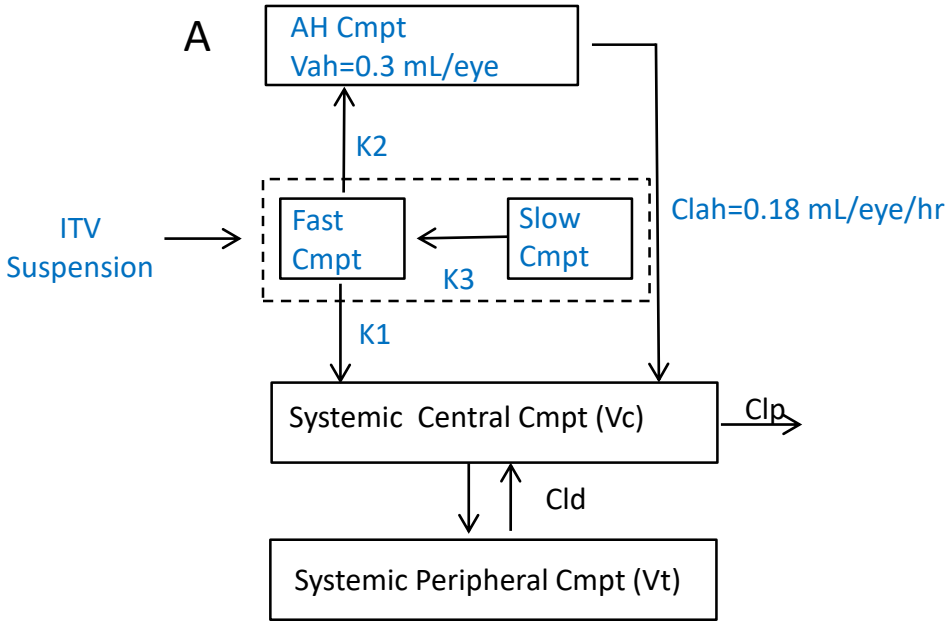
A
AH Cmpt
Vah=0.3 mL/eye
K2
ITV
Suspension
Fast
Cmpt
Slow
Cmpt
K3
Clah=0.18 mL/eye/hr
K1
Systemic Central Cmpt (Vc)
Clp
Cld
Systemic Peripheral Cmpt (Vt)

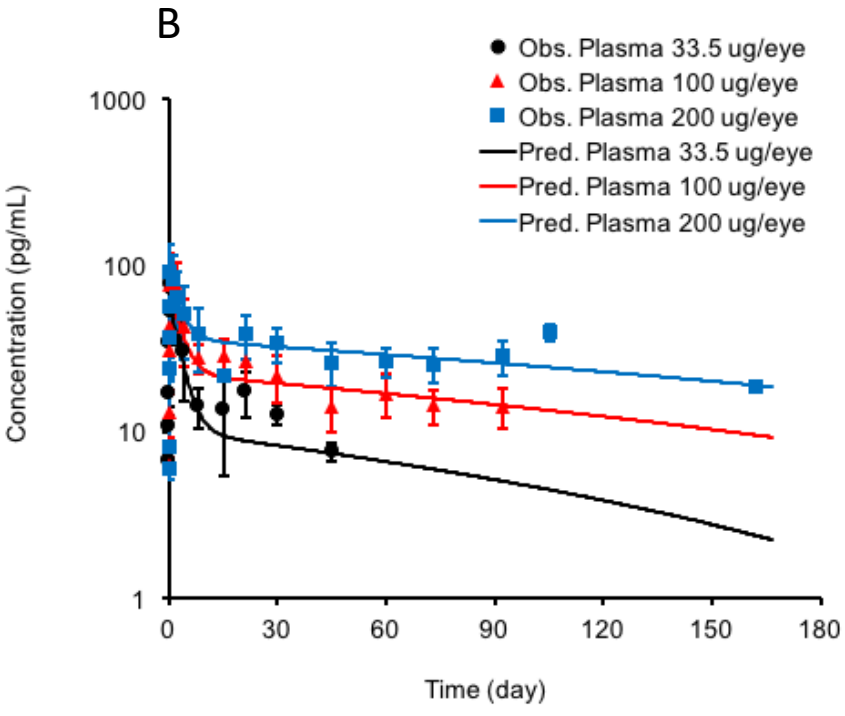
B
Obs. Plasma 33.5 ug/eye
Obs. Plasma 100 ug/eye
Obs. Plasma 200 ug/eye
Pred. Plasma 33.5 ug/eye
Pred. Plasma 100 ug/eye
Pred. Plasma 200 ug/eye
Concentration (pg/mL)
1000
100
10
1
0
30
60
90
120
150
180
Time (day)

Fig. 5

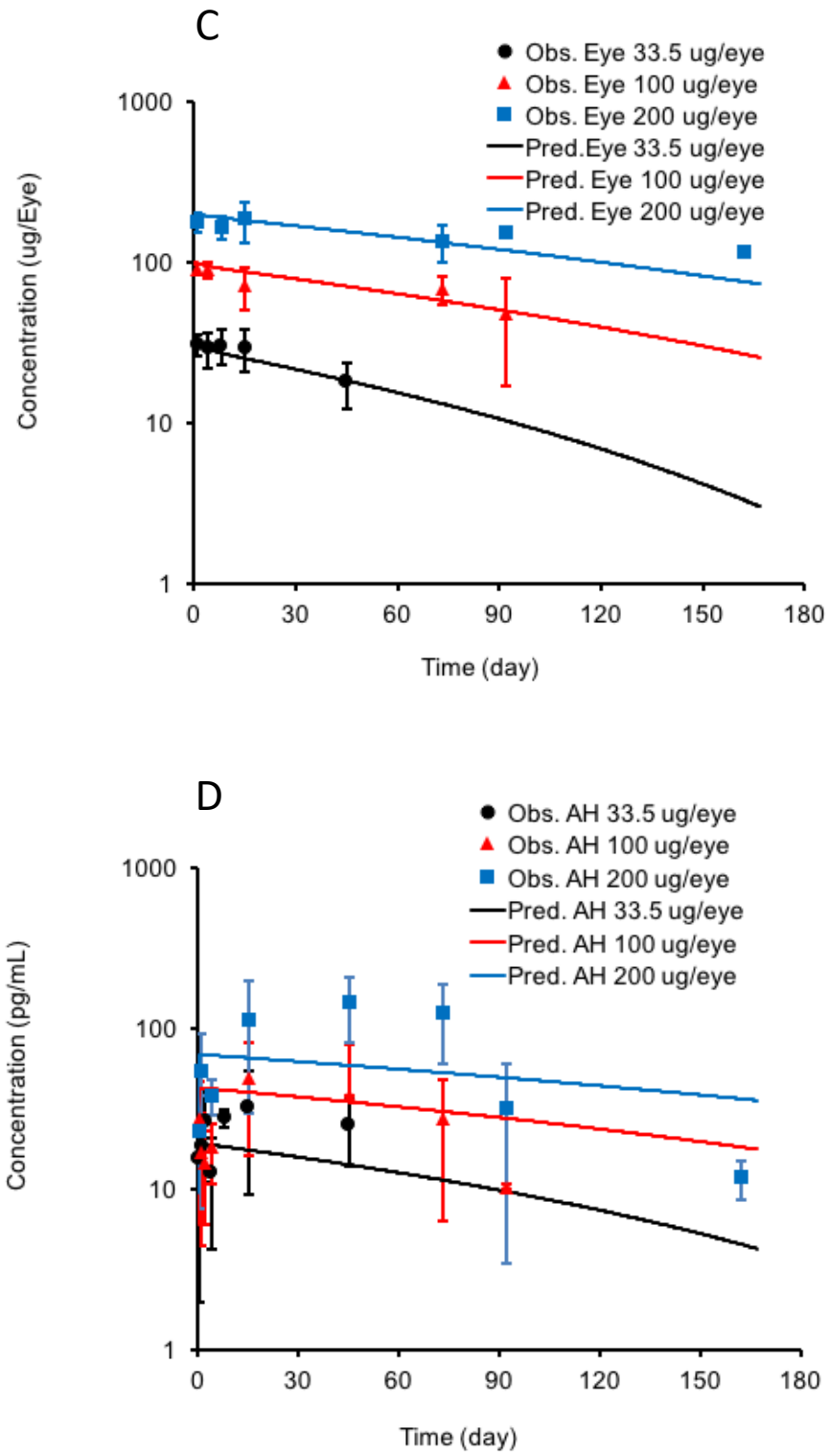
C
Obs. Eye 33.5 ug/eye
Obs. Eye 100 ug/eye
Obs. Eye 200 ug/eye
Pred.Eye 33.5 ug/eye
Pred. Eye 100 ug/eye
Pred. Eye 200 ug/eye
Concentration (ug/Eye)
1000
100
10
1
0
30
60
90
120
150
180
Time (day)
D
Obs. AH 33.5 ug/eye
Obs. AH 100 ug/eye
Obs. AH 200 ug/eye
Pred. AH 33.5 ug/eye
Pred. AH 100 ug/eye
Pred. AH 200 ug/eye
Concentration (pg/mL)
1000
100
10
1
0
30
60
90
120
150
180
Time (day)

Fig. 6 1000 µg/eye on day 30 (sagital section)

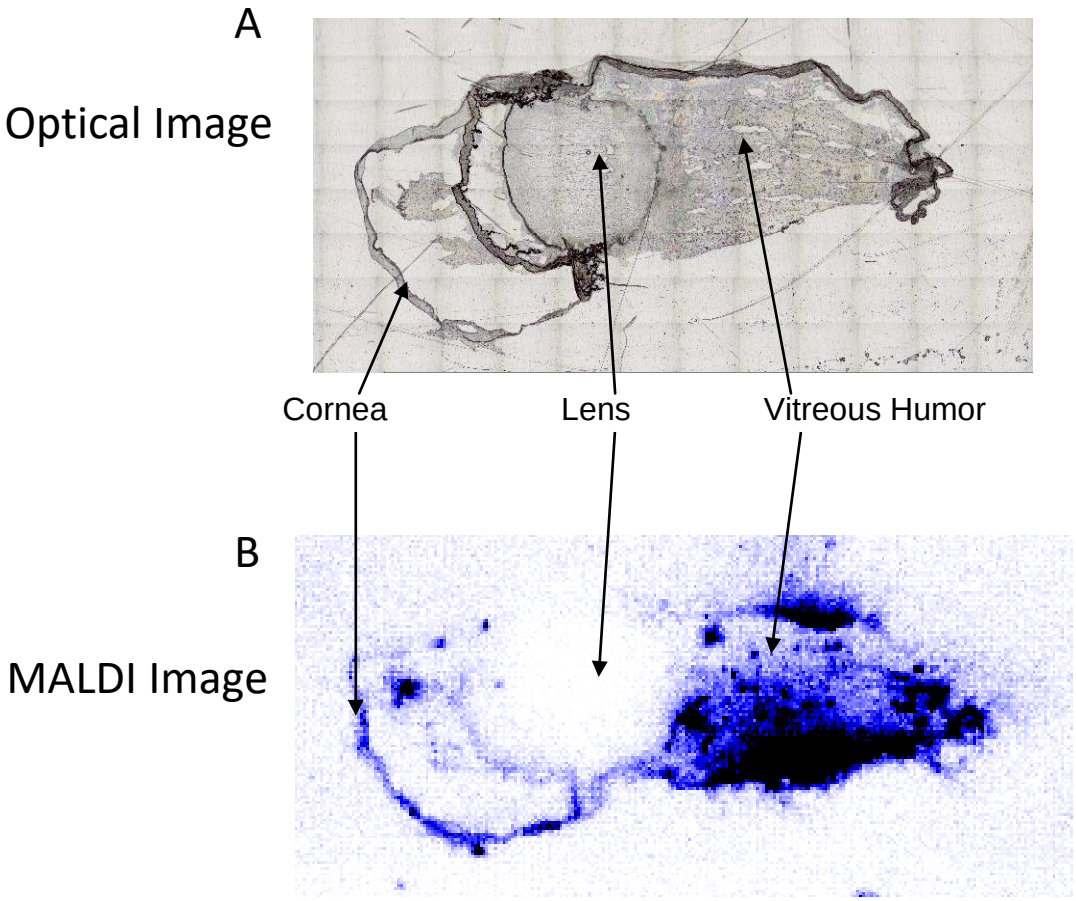

Fig. 7 150 µg/eye (frontal section)

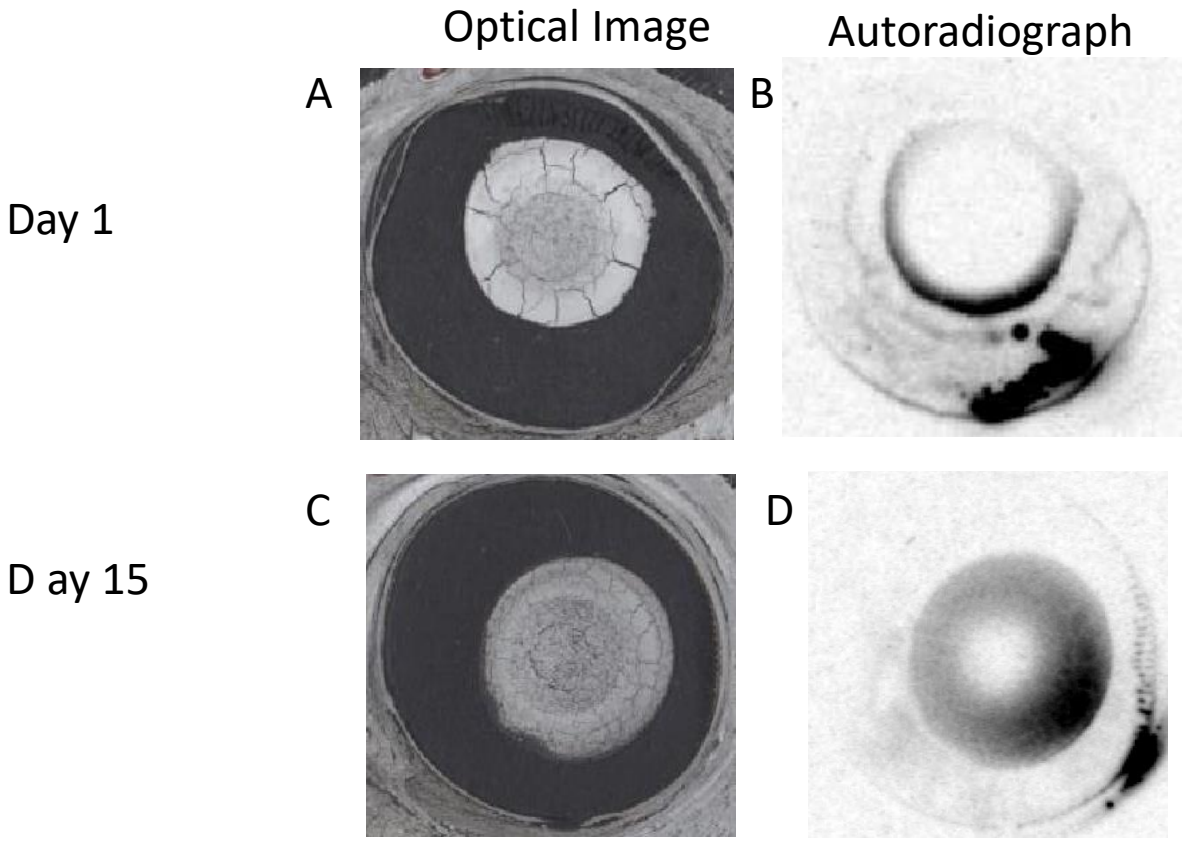

Fig. 8A 150 µg/eye on day 1 (sagital section)

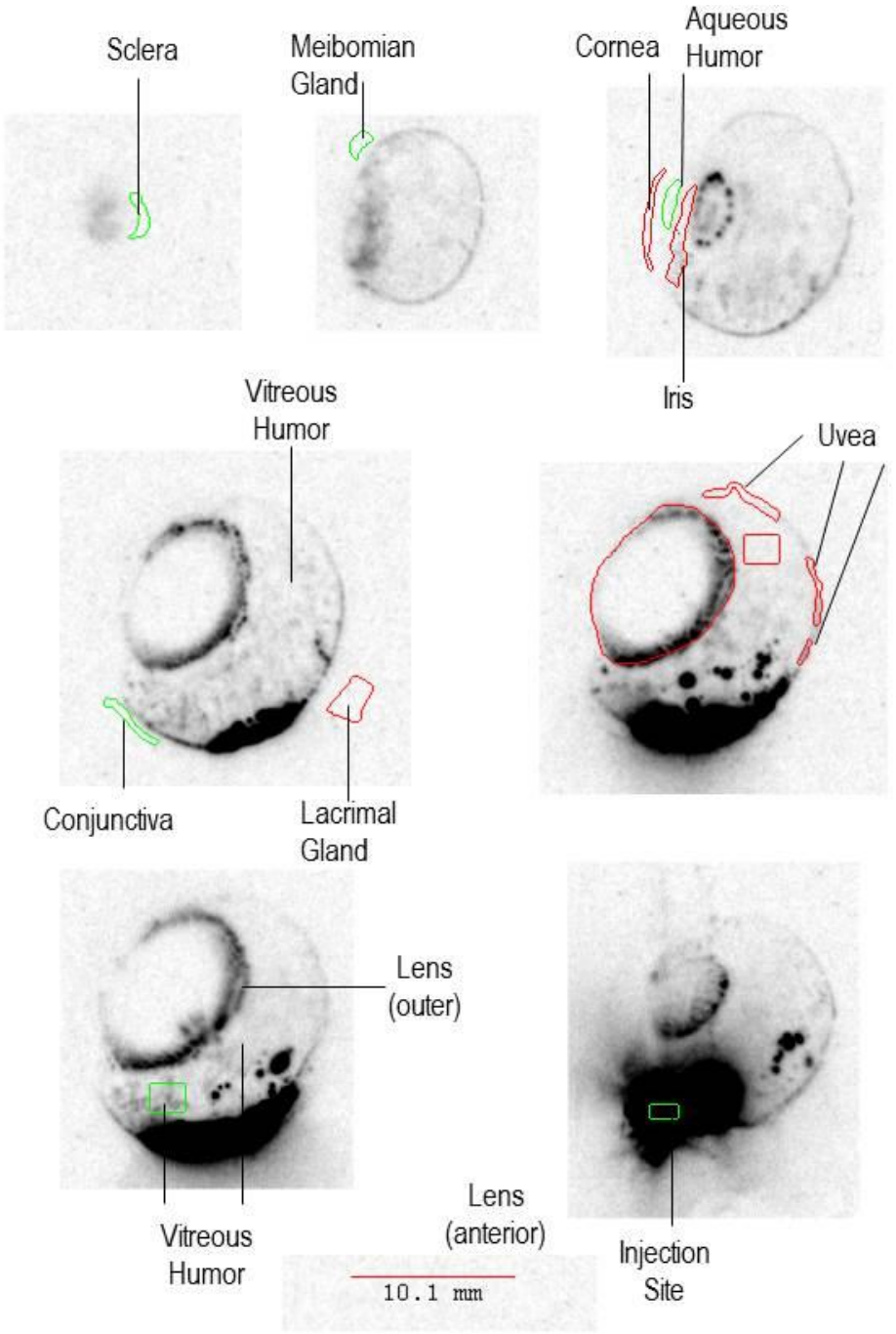

Fig. 8B 150 µg/eye on day 60 (sagital section)

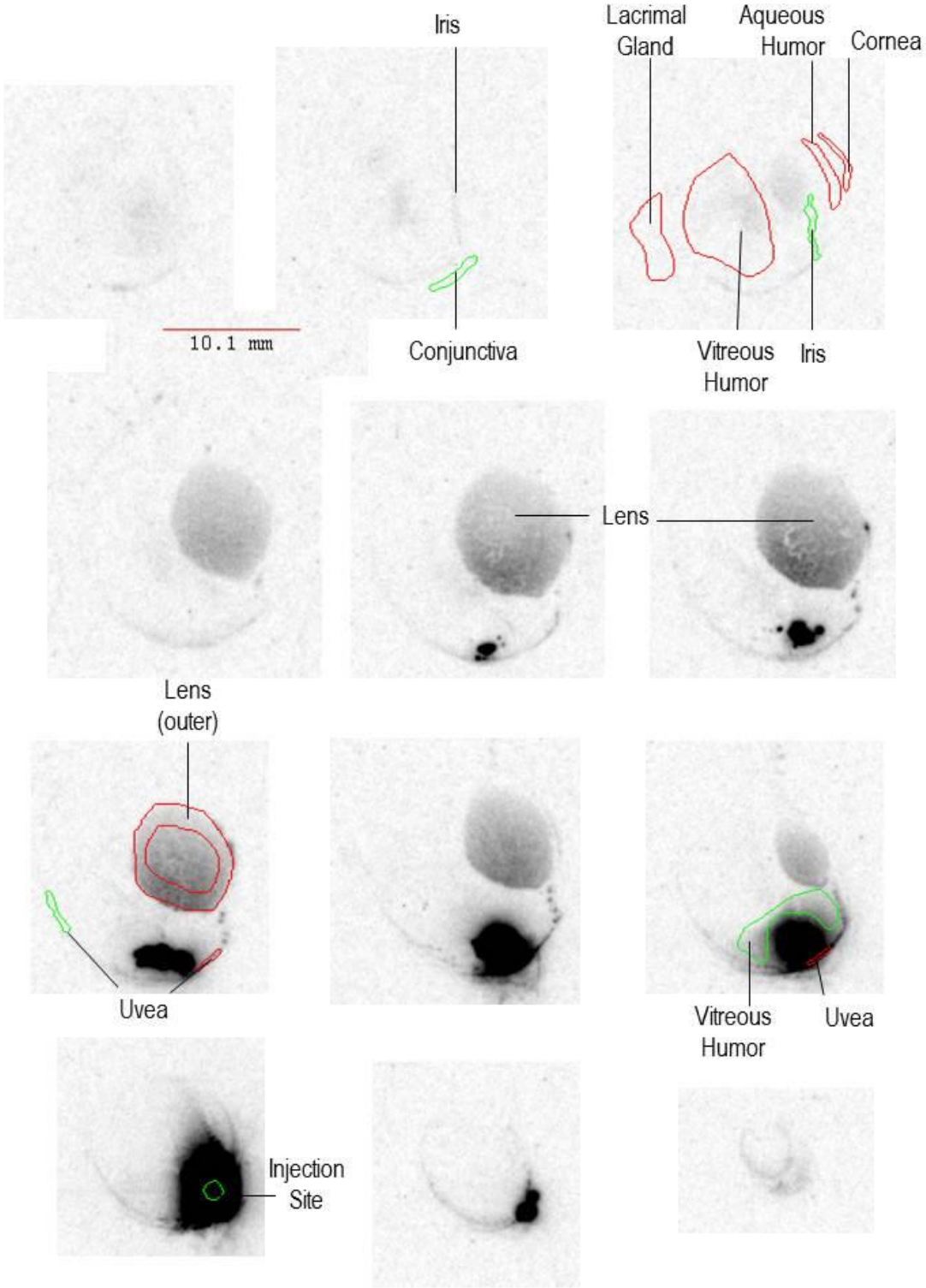

Fig. 9A

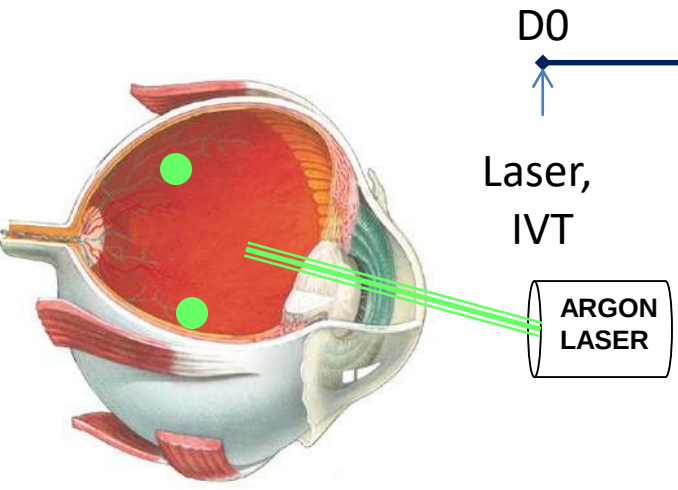
D0
D3
D7
D10
D14
Laser, IVT
IVT
IVT
IVT
Harvest
ARGON LASER

Fig. 9B

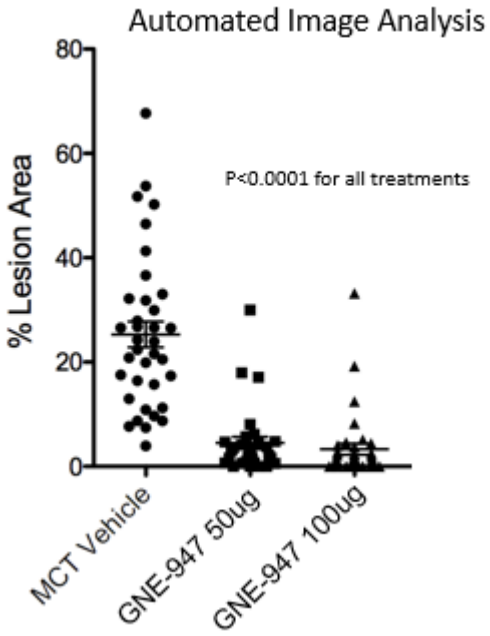
Automated Image Analysis
% Lesion Area
80
60
40
20
0
P<0.0001 for all treatments
MCT Vehicle
GNE-947 50ug
GNE-947 100ug